CHALMERS
UNIVERSITY OF TECHNOLOGY

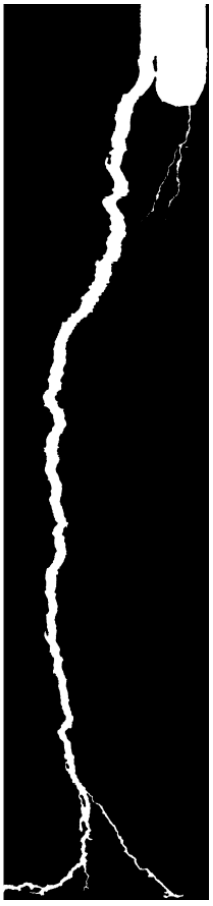

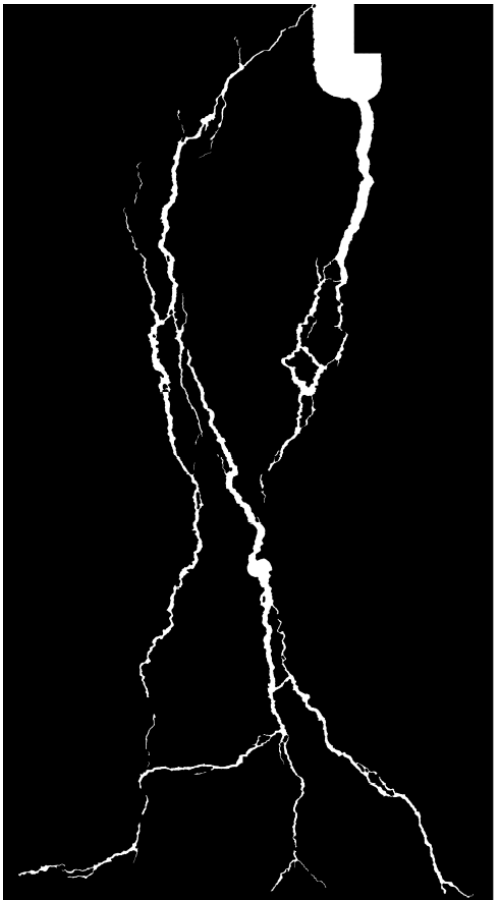

Hybrid Reinforcement Systems for Crack Width Control in Concrete Structures

Final Report – SBUF project number 12250

CARLOS GIL BERROCAL
INGEMAR LÖFGREN

Department of Architecture and Civil Engineering
Division of Structural Engineering
Concrete Structures
CHALMERS UNIVERSITY OF TECHNOLOGY
Gothenburg, Sweden 2018

Hybrid Reinforcement Systems for Crack Width Control in Concrete Structures

Final Report – SBUF project number 12250

CARLOS GIL BERROCAL
INGEMAR LÖFGREN

Department of Architecture and Civil Engineering
Division of Structural Engineering
Concrete Structures
Chalmers University of Technology
Göteborg, Sweden 2018

Hybrid Reinforcement Systems for Crack Width Control in Concrete Structures

Final Report – SBUF project number 12250

CARLOS GIL BERROCAL

INGEMAR LÖFGREN

Institutionen för arkitektur och samhällsbyggnadsteknik,
Chalmers Tekniska Högskola, 2018

Department of Architecture and Civil Engineering
Division of Structural Engineering
Concrete Structures
Chalmers University of Technology

SE-412 96 Göteborg

Sweden

Telephone: + 46 (0)31-772 1000

Cover:
Example of an unacceptably large crack in a concrete floor (top-left), image of a fractured section of a hybrid reinforced concrete element (bottom-left), and comparison of internal crack patterns in an element with conventional reinforcement (centre) and with hybrid reinforcement (right).

Table of Contents

Summary

In the present work, a literature study was conducted to evaluate the models included in current design codes regarding the calculation of crack widths in concrete structures, with and without fibre reinforcement. Moreover, an examination of the different approaches used to address restraint cracking in current design codes as well as a review of available state-of-the-art models for restraint cracking was performed. In parallel to the literature study, experimental tests were carried out where the cracking behaviour of tie-elements with hybrid reinforcement was investigated as a function of the fibre reinforced concrete properties, namely bond behaviour and residual tensile strength, which were assessed for a range of fibre dosages. Finally, an existing restraint cracking model based on a semi-empirical analytical relationship between the crack width and the stress at the reinforcement was further developed to include the effect of fibre reinforcement and was validated against experimental results, both from this study and reported in the literature.

Göteborg, May 2018

Carlos Gil Berrocal
Ingemar Löfgren

Exekutiv sammanfattning

Bakgrund
För vissa typer av betongkonstruktioner ställs krav på sprickbreddsbegränsning och kraven på maximal tillåten sprickvidd *w* kan variera från 0.05 till 0.4 mm med hänsyn till beständighet. Bro- och tunnel-konstruktioner, industrigolv samt vatten/vätsketäta konstruktioner är exempel på konstruktioner där det ställs eller kan ställas krav på sprickbredd. I normer och handböcker behandlas sprickbildning orsakad av mekaniska laster och konstruktörer är vana vid denna problemställning. Men eftersom normer och handböcker inte beaktar tvångslaster har konstruktörer ofta större svårigheter att beakta sprickbildning orsakad av t.ex. förhindrad krympning. Problemet är att med avseende på sprickbildning kan tvångslaster ha lika stor eller till och med större effekt än de mekaniska lasterna.

En sammanställning av skadeutredningar genomförd av CBI [1] visar att golv utgör cirka 20 % av skadefallen och av dessa är sprickor den vanligaste bristen (35 %) hos golv. Orsaken till dessa sprickor är de tvångskrafter som uppstår när betongen torkar ut och krymper vilket kan leda till en oacceptabel sprickbildning som inte är estetiskt tilltalande och som dessutom kan leda till beständighetsproblem och skapa en ohygienisk miljö. För att säkerställa golvens avsedda funktion måste sprickbildningen begränsa och detta kan åstadkommas med genomtänkt konstruktiv utformning och arbetsutförande. Exempelvis kan sprickor nästan helt undvikas genom att introducera rörelsefogar och skapa en låg friktion mot underlaget. Men detta kräver normalt mycket täta fogavstånd och helst en betong med mycket liten krympning. Önskas istället stora fogavstånd krävs det armering för att kontrollera sprickbildningen så att den hålls inom rimliga gränser. Konventionell armering medför dock en stor arbetsinsats. En möjlighet att reducera arbetsinsatsen är att kombinera fiberarmering med nätarmering, som leder till en ”kombinationsarmering” som är effektiv både konstruktivt, med hänsyn till sprickor, och vad gäller arbetsinsatsen. Ett ytterligare steg är att utnyttja modern betongteknologi och en självkompakterande fiberarmerad betong. Genom detta kan en industriell byggprocess, som är effektiv och resurssnål, skapas. I detta projekt har sprickbildning hos kombinationsarmerade tvärsnitt undersökt.

Allteftersom en betongplatta torkar ut krymper betongen och eftersom uttorkningen främst sker uppåt uppstår även krympskillnader över tvärsnittshöjden. Om plattan inte är fri att röra sig (fastlåst, sammangjuten eller på grund av friktion till underlaget) uppstår tvångskrafter och tvångsspänningar som kan leda till sprickor. Krympskillnaden över tvärsnittet leder dessutom till att plattan vill kröka sig. Om krökningen förhindras uppkommer dragspänningar på betongens ovansida och ytsprickor kan uppstå, om den inte förhindras kan kantresning ske.
Sprickor, orsakade av krympning och/eller belastning, måste begränsas eller elimineras eftersom breda och okontrollerade sprickor sällan accepteras i industrigolv. För krympsprickor finns det två möjligheter: (1) att försöka eliminera orsaken eller (2) att begränsa konsekvenserna. Eftersom orsaken är förhindrad krympning gäller det att minska tvånget eller betongens fria krympning såpass att de tvångsspänningar som uppkommer (med hänsyn till

krypning/relaxation) aldrig överstiger betongens draghållfasthet. Tvånget kan minskas genom att introducera glidlager under betongplattan eller genom att introducera täta fogavstånd. Betongens fria krympning kan minskas genom att reducera betongens vatten- och cementhalt, ha en stor stenhalt och stenstorlek, och med hjälp av krympreducerare. Konsekvenserna av sprickbildning kan begränsas med hjälp av armering. I Betongföreningens rapport om industrigolv, se Betongrapport nr 13 [5], anges maximalt tillåtna värden på betongens referenskrympning och i den högsta sprickbreddsklassen (klass I) anges att krympningen skall vara <0,5 mm/m. Att minska betongens krympning är gynnsamt men det kan vara svårt att reducera den i den omfattning som är nödvändig för att undvika sprickbildning. Detta kan bero på de krav som ställs på konsistens och maximal stenstorlek (t.ex. fullflyt med ärtor) eller att de delmaterial som finns tillgängliga (t.ex. grusmaterial) är vattenkrävande. I sådana fall är det möjligt att begränsa konsekvensen (sprickbredden) med hjälp av en lämpligt utformad armering. Eftersom armering är kostsamt och kräver en stor arbetsinsats bör den mängd som föreskrivs baseras på beräkningar. Men problemet är att dagens konstruktionsregler och handböcker (t.ex. EK 2 [34]) inte behandlar tvångskrafter vid beräkning av sprickbredder och för ”kombinationsarmerade” tvärsnitt (dvs. stång- och fiberarmering) saknas beräkningsmodeller helt. Men en beräkningsmodell för denna typ av sprickbildning för konventionellt armerade tvärsnitt har utvecklats av Engström [6] och har vidareutvecklats av Löfgren [4] för kombinationsarmerade tvärsnitt. Praktisk erfarenhet av kombinationsarmering, se Vitt [2], och beräkningar genomförda med beräkningsmodellen, se Betongrapport nr 13 [5], har påvisat att kombinationsarmering är en mycket effektiv sprickarmering och att det är möjligt att minska mängden konventionell armering med upp till 50%.

Slutsatser

I rapporten har sprickbildning orsakad av tvångskrafter i kombinationsarmerade betongelement undersökts, både genom en omfattande litteraturstudie och genom att utföra experiment. Avsikten har varit att utveckla beräkningsmodeller och riktlinjer för dimensionering men också för att undersöka och fastlägga hur effektiv kombinationsarmering är för att kontrollera sprickbildning.

Baserat på resultaten i denna undersökning kan följande slutsatser dras:

- Beräkning av sprickbredd enligt gällande normer och rekommendationer är främst begränsat till lastberoende sprickor. Men förenklat dimensioneras armeringsmängden utifrån att begränsa armeringens diameter och spänningen beroende på sprickbreddskrav.
- Det finns en rad olika modeller föreslagna för hur sprickbredden kan beräknas för konstruktioner utsatta för tvång. I de flesta modellerna introduceras ofta förenklingar, t.ex. att armeringens vidhäftnings-glidningssamband är konstant, vilket kan leda till begränsningar vad gäller möjligheten att prediktera sprickbredder där vidhäftningsegenskaperna varierar.
- För kombinationsarmerade konstruktionselement finns några modeller föreslagna vad gäller last beroende sprickor och dessa är baserade på befintliga modeller för konventionell armering. Men för sprickbildning orsakad av tvång verkar beräkningsmodeller saknas.

- De försök som genomförts påvisar att tydligt att fiberarmering har en mycket gynnsam inverkan på sprickbildningsprocessen. I enaxiella dragförsök undersöktes inverkan av ökande fiberdosering (från cirka 0,25 till 1,0 vol.-%) på residualdraghållfastheten och denna ökade från 10 % till 8 0% av betongens draghållfasthet för en sprickbredd upp till 1 mm. Den ökade residualdraghållfastheten resulterade i reduktion av medelsprickbredden, hos kombinationsarmerade dragstag, av upp till 55 %. I de försök som genomfördes för att undersöka fibrernas inverkan på armeringens vidhäftnings-glidningssamband visade att de inte hade någon inverkan på sambandet upp till max vidhäftningsspänning, men att de påverkade residualvidhäftningsspänningen då armeringen började att glida.
- En befintlig analytisk modell för tvångssprickor har vidareutvecklats för att beakta inverkan av fiberarmeringen så att denna också kan användas för kombinationsarmering.
- Den föreslagna och modifierade modellen, som ger ett samband mellan medelsprickbredd och armeringsspänning, stämmer väl överens med de försök som genomförts man också med andra analytiska modeller. Dock bör det beaktas att det var en relativ stor spridning i sprickbredd mellan enskilda sprickor, särskilt vid höga påkänningar.
- Utifrån att analysera försök som genomförts av andra kunde det påvisas att den föreslagna beräkningsmodellen kunde med god överensstämmelse prediktera antalet sprickor i betongplattor utsatta för förhindrad krympning. Överensstämmelsen mellan medelsprickbredd och armeringspåkänning var också rimlig och visar att modellen har möjlighet att prediktera spickbildning och sprickbredder.

Förslag på fortsatta studier

I litteraturen finns omfattande försöksresultat som beskriver effekten av fiberarmering på spickbredd och sprickavstånd i kombinationsarmerade dragstag utsatta för dragbelastning. Men försöksresultat för sprickbildning orsakad av förhindrad rörelse saknas och därför finns det ett behov för sådana undersökningar.

Den föreslagna beräkningsmodellen för kombinationsarmerade tvärsnitt, i sin nuvarande form, baseras på att fibrernas inverkan på residualdraghållfastheten är känd. För att bestämma residualdraghållfastheten måste därför försök genomföras för att denna materialegenskap ska kunna bestämmas. Vanligtvis karakteriseras fibrernas inverkan genom att genomföra balkböjningsförsök och där resultatet omvandlas till residualdraghållfasthet. Men i idealfallet skulle en modell och ett samband utvecklas för att också kunna prediktera residualdraghållfastheten utifrån typ av fiber, dess geometri, dosering, fiberorientering och betongens egenskaper.

Den föreslagna beräkningsmodellen för tvångssprickor kunde endast jämföras och valideras för ett begränsat antal försök och dessa var dessutom begränsade till enbart konventionellt armerade tvärsnitt. Därför finns det ett behov av ytterligare validering gentemot försöksresultat både för konventionellt och kombinationsarmerade tvärsnitt.

Det är också önskvärt att undersöka produktions- och livscykelkostnaderna för olika armeringslösningar för olika sprickbreddskrav. Detta för att få ett underlag gällande kombinationsarmeringens ekonomiska möjlighet och potential.

Preface

The present work was carried out by Dr. Carlos Gil Berrocal and Adj. Prof. Ingemar Löfgren at Thomas Concrete Group AB in collaboration with the division of Structural Engineering, Concrete Structures research group at Chalmers University of Technology, between 2010 and 2017. The main responsible for the experimental tests carried out within the present work was Dr. Anette Jansson. The project has been funded by SBUF according to the project number 12250 ("*Kombinationsarmering för sprickbreddsbegränsning*"). A project and reference group have consisted of: Pär Åhman (BI), Hans Hedlund (Skanska), Jonas Magnusson (NCC), Peter Mjörnell (Bekaert), Rolf Jonsson (Wästbygg), Johan Silfwerbrand (KTH).

1. Introduction

1.1. Background and motivation

For certain reinforced concrete structures, crack control is often necessary in order to meet specific requirements regarding appearance, serviceability and durability. Bridge and tunnel constructions, industrial floors as well as water retaining structures are examples of structures where crack width limitations may be required. The maximum crack width, $w_{max,}$ that is considered acceptable in current design codes and recommendations depends on the function of the structure, its design service life and the environmental conditions to which it is exposed, resulting in acceptable crack widths that can range from 0.05 to 0.4 mm.

Today, the tools provided in design codes to ensure that crack width limitations are satisfied are mostly empirical or semi-empirical models derived for mechanically-induced cracks and calibrated for a number of laboratory experimental tests. However, cracks in reinforced concrete structures may appear due to causes other than externally applied loads. As a concrete element dries out, the loss of moisture in the concrete due to evaporation causes drying shrinkage, which results in a certain need of deformation. Similarly, negative variations of the ambient temperature can also lead to imposed deformation requirements on the structures. If the longitudinal movement caused by shrinkage or thermal contraction is restrained, tensile stresses appear in the concrete which can lead to cracking. According to a compilation of damage investigations conducted by CBI [1], flooring accounts for about 20% of the damage occurrences, out of which cracks are the most common deficiency (35%). The reason for these cracks are the restraint forces that appear when the floor dries out and shrinks, leading to unacceptably large cracks that are may impair its aesthetical appearance and its durability or functionality.

To ensure the intended function of the floor, cracking must be limited, which can be accomplished with thoughtful design and workmanship. For shrinkage cracks there are two main approaches: (1) attempting to eliminate the cause or (2) trying to limit the consequences. Since the main cause of restraint cracking is prevented shrinkage movement, the problem can be addressed by either drastically reducing the free shrinkage of the concrete so that the need for deformation is decreased or minimizing the external restraint forces, so that the tensile stresses that develop never exceed the tensile strength of the concrete. The free shrinkage of the concrete can be reduced by decreasing the water and cement content, having a large aggregate size or by means of a shrinkage reducer agent. The restraint forces, on the other hand, can be minimized by introducing closely spaced expansion joints or creating a low friction surface against the substrate. Reducing concrete shrinkage is beneficial, but it cannot always be feasible to decrease it to the point where cracking is prevented. This may depend on the requirements for consistency and maximum aggregate size or that the available material (e.g. gravel) has a high water absorption capacity. In such cases, it is possible to limit the impact (crack width) by means of a suitably designed reinforcement.

However, the placing of conventional reinforcement is a costly, tedious and labour-intensive task. The use of fibre reinforced concrete, on the other hand, has been shown to be an effective means of controlling crack widths, even in elements containing traditional rebar. Practical experience has revealed that using fibre reinforcement may enable a reduction of conventional reinforcement of up to 50% [2]. Thus, an opportunity to create a synergistic effect arises from the combination of fibre and conventional reinforcement, resulting in a "hybrid reinforcement" that is both effective with respect to crack control and efficient in terms of labour effort. A further step could involve the utilization modern concrete technology and a self-compacting mix design. Thus, an industrial construction process that is both effective and resource-efficient could be created.

The main current difficulty for the implementation of such a construction process is that even though restraint loading can have a similar or even a greater impact with respect to cracking than mechanical loading, current design codes do not specifically take into account restraint loads. This is partially due to the fact that today there is not a widely acceptable model for crack width calculation in reinforced concrete elements subjected to restraint cracking. Consequently, the way current design codes address the problem of restraint cracking usually consist in limiting the stress level at the reinforcement by providing minimum reinforcement amounts while simultaneously limiting the size of the bar diameter used.

A calculation model for restraint cracking in conventionally reinforced cross-sections has been developed by Engström [3] and adapted by Löfgren [4] for hybrid-reinforced cross-sections, see also [5]. This report investigates cracking in hybrid reinforced cross-sections with the aim of developing practical useful recommendations and calculation tools to provide support in the design and execution phase, as well as in material selection, of concrete floors. The existing model is further developed and its potential for the design of structures subjected to restraint forces with respect to crack width calculations, for both conventionally reinforced and hybrid reinforced concrete, is shown.

1.2. Aim and objectives

The purpose of the project is to provide a basis for recommendations on the design and execution, as well as to demonstrate the effectiveness of hybrid reinforcement for concrete structures, with particular interest in concrete floors. The successful implementation of the project is expected to lead, in the long-term, to increased profitability and reduced work-related injuries through optimized and simplified reinforcement management at the construction site. An additional goal is to reduce the number of complaints due to unacceptable cracking as a result of improved cracking.

These goals will be achieved through experimental studies in the laboratory, investigation of the cracking behaviour of hybrid reinforced elements and a comparison of the results with theoretical calculations.

Consequently, the objectives of this report are:

- To review and report the way in which restraint cracking is addressed in current design codes and recommendations as well as in state-of-the-art analytical models.
- To investigate, experimentally, cracking in hybrid reinforced concrete elements as well as the effect of fibres on relevant material properties, such as the residual tensile strength and the bond-slip relationship.
- To further develop an existing calculation model to adapt it to hybrid reinforced cross-sections and validate it with the aid of available experimental results.

1.3. Methodology and Outline of the report

A literature study was conducted to evaluate the models included in current design codes regarding the calculation of crack widths in concrete structures, with and without fibre reinforcement. Moreover, an examination of the different approaches used to address restraint cracking in current design codes as well as a review of available state-of-the-art models for restraint cracking was performed. In parallel to the literature study, experimental tests were carried out where the cracking behaviour of tie-elements with hybrid reinforcement was investigated as a function of the fibre reinforced concrete properties, namely bond behaviour and residual tensile strength, which were assessed for a range of fibre dosages. Finally, an existing restraint cracking model based on a semi-empirical analytical relationship between the crack width and the stress at the reinforcement was further developed to include the effect of fibre reinforcement and was validated against experimental results, both from this study and reported in the literature. The outline of the report includes:

Section 1 provides the background and motivation of the project, the aim and objectives as well as the methodology.

Section 2 introduces the fundamental knowledge necessary to establish the theoretical framework on which this project has been developed.

Section 3 reviews and briefly discusses the different available methods for the calculation of the crack with in conventionally and hybrid reinforced concrete. Subsequently, an analytical model is presented and further developed.

Section 4 presents an overview of the experimental programme including the description and main results of the different experiments carried out as well as the description of experiments performed by others which are used to validate the analytical model.

Section 5 includes a comparison between the predictions obtained with the proposed analytical model and the experimental results, as well as with other analytical models.

Section 6 summarizes the most important findings of the study and the need for further research.

2. Theoretical framework and literature study

2.1. Restraint cracking in reinforced concrete structures

- *Stress-independent strain in concrete elements*

The strain to what concrete elements are often subjected can be caused by actions of very different origin including externally applied loads, imposed deformations, thermal gradients, shrinkage, chemical reactions occurring inside the concrete, etc. Depending on their nature, strain can be classified as either stress-dependent or stress-independent.

Stress-dependent strain occurs when the concrete is loaded, i.e. when it is subjected to an external pressure that results in the development of stresses in the material. Upon loading, an instantaneous strain develops, referred to as *elastic strain* ($\varepsilon_{c,el}$), which is proportional to the stress applied. However, additional strain can develop under sustained loading due to creep effects. *Creep strain* ($\varepsilon_{c,creep}$) develops with time at a decreasing rate until it approaches a nearly constant value in the long-term, see Fig. 2.1. The most relevant factors influencing the creep strain are the maturity of the concrete when the load is first applied and the magnitude and duration of the loading [6]. The total stress-dependent strain at a time t for a concrete element subjected to a constant stress σ_c applied at a concrete age t_0 can be expressed as the sum of the elastic and creep strains according to Eq. 2.1 [7]:

$$\varepsilon_c(t) = \varepsilon_{c,el} + \varepsilon_{c,creep}(t) = \frac{\sigma_c}{E_c} + \varphi(t,t_0)\frac{\sigma_c}{E_c} = \left(1 + \varphi(t,t_0)\right)\frac{\sigma_c}{E_c} \quad (2.1)$$

where E_c is the modulus of elasticity of the concrete and $\varphi(t,t_0)$ is the creep coefficient.

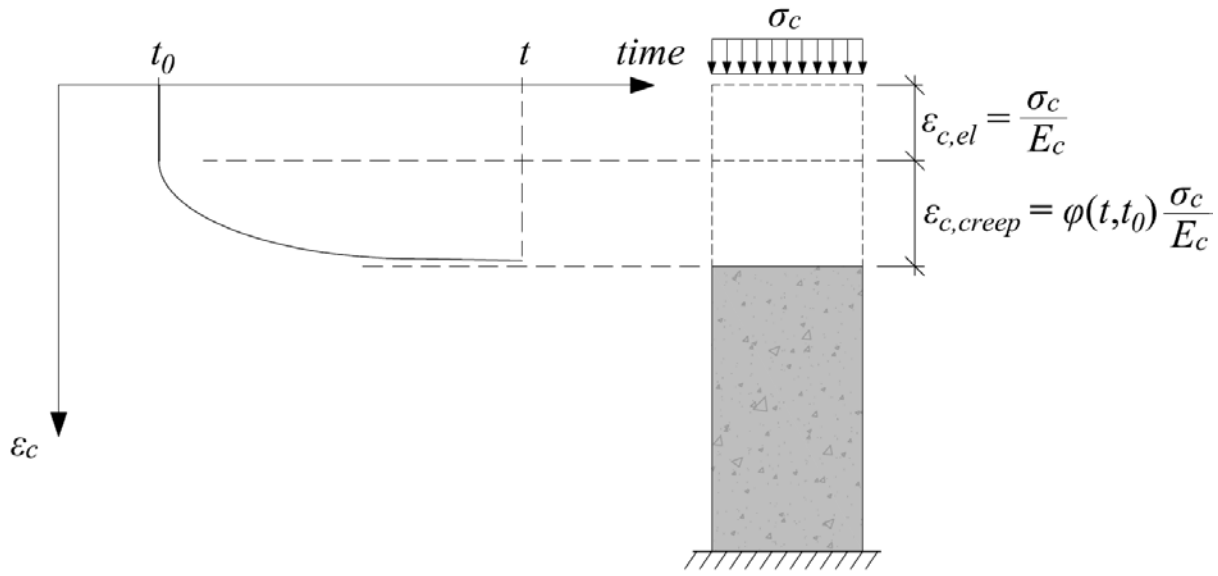

Figure 2.1 Time-evolution of the deformation in concrete subjected to a constant stress

Stress-independent strain, on the other hand, is the strain that results in the deformation of the concrete without the need of applying an external load. The most common types of stress-independent strain are:

a) Thermal strain
b) Shrinkage strain

Thermal strain (ε_T) are caused by a change in the temperature of the material and it can affect both concrete and steel. Thermal strain depends on the magnitude of the temperature change, ΔT, and on the coefficient of thermal expansion of the material, α_T, and it can be expressed by Eq.2.2 as:

$$\varepsilon_T = \alpha_T \cdot \Delta T \tag{2.2}$$

The value of the thermal expansion coefficient of concrete is commonly taken as $\alpha_{cT} = 10 \cdot 10^{-6}$ $°C^{-1}$ although it might slightly vary depending on the type of aggregate used. The thermal expansion coefficient of steel is closer to $\alpha_{sT} = 12 \cdot 10^{-6}$ $°C^{-1}$ but, in practice, the same approximate value as for concrete is assumed, i.e. $\alpha_{sT} = \alpha_{cT} = 10 \cdot 10^{-6}$ $°C^{-1}$.

Shrinkage strain (ε_{cs}) is caused by a change in the amount of water in the concrete pore network and, unlike thermal strain, it affects the concrete but not the steel. It is important to differentiate between plastic shrinkage and drying and autogenous shrinkage. The former occurs in the wet concrete before setting, whereas the former two take place when the concrete is already hardened [8]. Similar to creep, shrinkage strain develops with time until it reaches a nearly constant value after a long period of time. Shrinkage strain, ε_{cs}, is often considered as the sum of two components coming from different mechanisms, namely the drying shrinkage strain, ε_{cd}, and the autogenous shrinkage strain, ε_{ca}, which can be written as Eq.2.3. For normal concrete, the final shrinkage strain typically varies between $400 \cdot 10^{-6}$ to $700 \cdot 10^{-6}$ but it can vary between values of $100 \cdot 10^{-6}$ and $1000 \cdot 10^{-6}$, depending on several factors.

$$\varepsilon_{cs}(t) = \varepsilon_{cd}(t) + \varepsilon_{ca}(t) \tag{2.3}$$

Drying shrinkage is related to the exchange of moisture between a concrete element and its surrounding environment, which means that in theory swelling due to water absorption is also possible, although far less common. All the factors that affect the drying of concrete play an important role in the drying shrinkage component, including the initial water content in the concrete, factors that control the pore network characteristics such as the water-cement ratio and type of binder used, the exposed surface to volume ratio of the concrete element under consideration and the ambient conditions, being especially important the relative humidity.

As the drying process depends on the transport of moisture inside the concrete, the full development of the shrinkage strain can be a very slow process. The role of the element's size on the time required to achieve the final shrinkage strain should be highlighted, which can vary

from 1 year to 100 years, by increasing the thickness of a wall from 0,1 m to 1 m [9]. Moreover, it should be noted that in thick members, the shrinkage strain will not be uniformly distributed across the section. Conversely, the areas located close to an exposed surface will experience a quicker loss of moisture and will, consequently, be subjected to a greater shrinkage strain than inner zones which remain moist, giving rise to a non-linear distribution of the shrinkage strain.

The autogenous component of the shrinkage strain, on the other hand, can be attributed to the amount of water that is consumed by the chemical reactions taking place during the hydration process of cement after the initial setting of the concrete. This mechanism occurs during the early days after the casting and takes place without an exchange of moisture with the surrounding environment. This component of the shrinkage is more significant in the inner zones of elements made of concrete with a low *w/c* ratio, where the transport of moisture towards the surface is a very slow process.

- *Need for deformation and restraint*

When a concrete element is subjected to stress-independent strains, a certain need for deformation arises, which depends on the distribution of strains across the section of the element. In reality, the variation of strain across a section is never perfectly linear but, in practice, the strain distribution can be sometimes considered as uniform or linear. For instance, in thin elements where both sides are subjected to similar conditions, a uniform strain distribution may be considered as a satisfactory approximation of the real strain distribution. When the conditions at either side of the element differ significantly, the stress-independent strain at the edges of the section will also become different, thereby resulting in a skew strain distribution, which may be approximately linear. Note that for the case of uniform strain distribution, the resulting need for deformation is also a uniform axial displacement of the whole section whereas for linearly varying strains, the total deformation required consists of an axial displacement and a rotation.

When the development of stress-independent strains give rise to the need for deformation of a concrete element, that deformation might be partially or totally prevented by the existence of external and/or internal restraints. Therefore, depending on how the need for deformation in an element is satisfied, three different scenarios can be distinguished:

a) No restraint: the need for deformation is fully satisfied and all movements are allowed.
b) Total (or full) restraint: movements are completely prevented and consequently the need for deformation is not satisfied. In this case, stress-dependent strains develop of equal magnitude than the stress-independent strains but opposite sign. Stress-dependent strains result in the development of stresses and consequently of restraint forces, which depend on the stiffness of the element.
c) Partial restraint: the need for deformation is only partially satisfied meaning the restraint allows for a certain movement. In this case, stress-dependent strains also develop although they are smaller than for the total restraint case. On the other hand, the magnitude of the restraint forces in partially restrained members depends on the stiffness of both the member itself and the restraint elements.

In practice, the two first cases are only ideal situations assuming friction-free supports or infinitely rigid boundaries. Realistic restraints will often lay within the third case, although they can be close to the extreme ones. In order to quantify the degree of movement allowed by a restraint, the concept of degree of restraint, R, can be introduced, where the ideal cases of no restraint and total restraint would have values for the degree of restraint of 0 and 1, respectively. Accordingly, the degree of restraint can be defined as:

$$R = \frac{Restrained\ deformation}{Total\ need\ for\ deformation} \tag{2.4}$$

If a concrete element is subjected to shrinkage or to a negative temperature increment, a certain need for shortening arises. If the deformation of the element is either partially or fully restrained, then tensile stresses will develop in the concrete. Depending on the magnitude of the stress-independent strain and the degree of restraint at the boundaries, the stress level can reach the tensile strength of the concrete resulting in cracking.

- *The cracking process in reinforced concrete members*

The investigation of the cracking process in reinforced concrete and many of the expressions commonly used today to calculate the crack width in reinforced concrete members are based on the study of a thin prismatic concrete specimen reinforced with a single centric bar and subjected to uniaxial tension as depicted in Fig. 2.2.

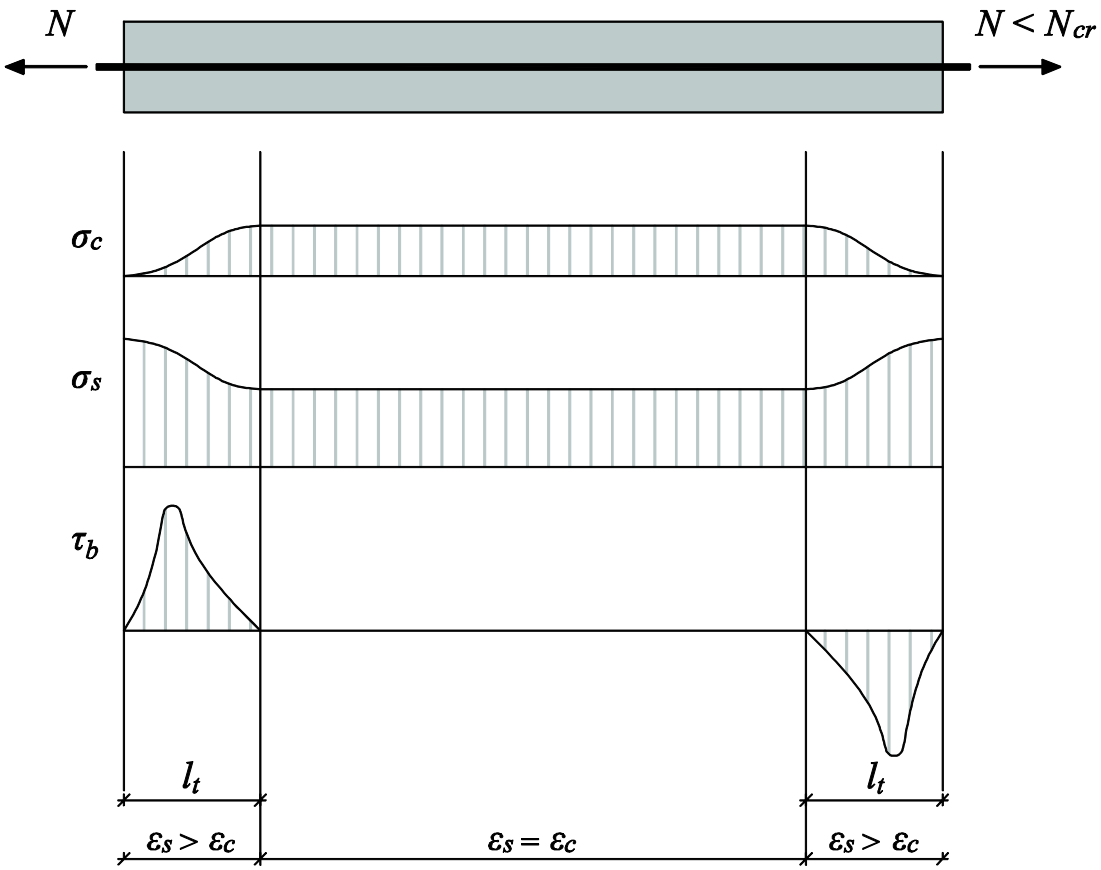

Figure 2.2. A thin prismatic reinforced concrete member subjected to a tensile load below the cracking load and the corresponding distributions of tensile stress in the concrete, in the steel and bond stress at the steel-concrete interface, after Engström [6].

When the reinforcement bar in the specimen from Fig. 2.2 is subjected to a tensile load pulling from the ends of the specimen, its natural tendency is to elongate. However, due to the existing bond between the steel bar and the surrounding concrete, the bar is not able to move freely. Instead, bond stresses develop near the ends of the specimen, with an associated slip, which decrease the normal stress in the bar and increase the normal stress in the concrete. This load transfer from the bar to the concrete occurs along a certain length commonly referred to as the transmission length, which greatly depends on the bond properties of the steel-concrete interface. In the central region of the specimen, beyond the transmission length, compatibility exists between the deformations of the reinforcement bar and the concrete, hence no relative displacement takes places and subsequently no bond stresses are generated.

When the magnitude of the applied load is increased, the transmission length also increases. The transmission length keeps increasing with the load until the concrete normal stresses in the mid-region of the specimen reach the tensile strength of the concrete. At that point, the extension of the transmission length has reached its limit, $l_{t,max}$, since any further increase of the load would result in the formation of a crack. When the first crack appears, the cracked section divides the specimen into two parts, each of which behaves as individual members loaded in

tension from their respective bar ends. Since the concrete is no longer able to carry normal stresses through the crack, the concrete on each side of the cracks tends to shorten thereby slipping relative to the reinforcement bar and creating new transmission zones with development of bond stresses on each side of the crack.

Theoretically, multiple cracks could form without needing a further increase of the applied load. In practice, due to variations in the local properties of the concrete and the existence of small imperfections distributed along the specimen, the actual cracking load is not constant for every section of a concrete element. Therefore, the first crack is likely to occur at a section with a slightly weaker cracking resistance than other sections in the neighbouring zones, and the formation of subsequent cracks requires a small load increment.

The formation of new cracks continues as long as the distance between two consecutive cracks is larger than twice the maximum transmission length. If the distance between two cracks is shorter, the built-up stresses in the concrete will not reach the tensile strength and therefore a new crack cannot form. This point determines the end of the "crack formation" phase. A further load increment will not result in new cracks but it will cause the already formed cracks to become wider while the stress at the reinforcement will continue increasing until the yielding strength is eventually reached.

- *Effect of loading and boundary conditions*

The cracking behaviour of a reinforced concrete member may vary depending on how the load is applied and also on the existing boundary conditions. To illustrate this concept, a thin prismatic reinforced concrete member is subjected to direct tension in three different ways, as schematically depicted in Fig. 2.3:

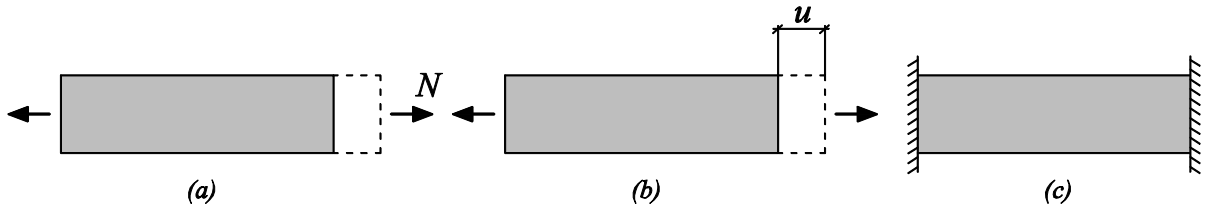

Figure 2.3. Thin prismatic reinforced concrete member subjected to tensile loading, a) load-control, b) displacement-control, c) restrained shrinkage, after Engström [6].

In the first two cases, the concrete member shares the same boundary conditions, i.e. no restraints exist and the member can deform freely. However, in the first case the load is prescribed and the concrete member deforms freely whereas in the second case the deformation of the member is imposed and the resulting tensile load varies according to the stiffness of the member. In the third case the ends of the member are fully fixed, i.e. a total restraint exists, and the tensile loading arises from the stress-dependent strain that appears to compensate the development of stress-independent strain stemming, for instance, from shrinkage. Similar to the case with imposed deformation, the magnitude of the tensile load in a restrained member will depend on the stiffness of the member.

Whenever a new crack is formed in the reinforced concrete member the overall stiffness of the member decreases regardless of the loading or boundary conditions. However, the evolution of the load-displacement relationship is essentially different for the three cases discussed above, as shown in Fig. 2.4.

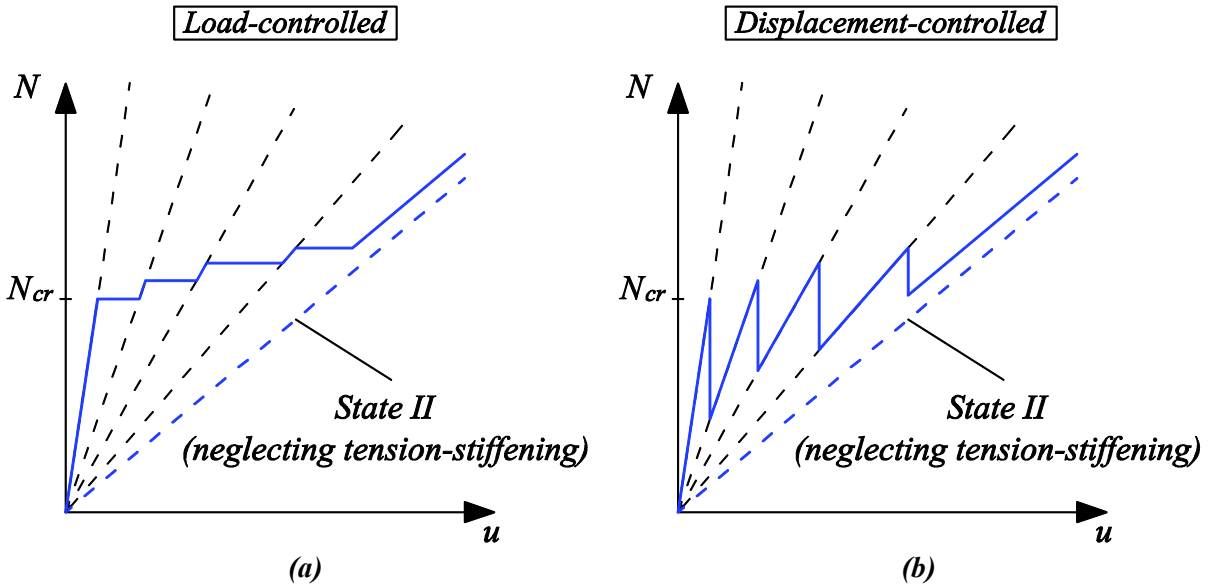

Figure 2.4. The load-displacement relationship of a reinforced concrete member subjected to tensile loading, (a) under load-controlled conditions and (b) under displacement-controlled conditions, after [10].

For a load-controlled member as in Fig. 2.3a, a sudden deformation of the member occurs upon crack formation under a virtually constant load level as a result of the decreased stiffness, see Fig. 2.4a. Conversely, when a new crack is formed in a displacement-controlled member, the achieved displacement just prior to cracking remains unchanged but the loss of stiffness results in a reduction of the load, see Fig. 2.4b. The initiation of subsequent cracks requires a slightly larger load than that achieved for the previous ones. Further loading and deformation of the member develops according to its new reduced stiffness until a new crack is formed. This process is successively repeated, with a corresponding reduction of the overall stiffness for each new crack, until the member reaches the stabilized cracking stage where no new cracks can appear.

In the case of the tensile loading due to restrained shrinkage strain, an unequivocal load-displacement relationship does not exist, since the elongation of the member is partly prevented (depending on the degree of restraint). Nevertheless, since the shrinkage of concrete develops over time, the evolution of the restraint force with time can be represented, as shown in Fig. 2.5(b). It can be observed that the evolution of restraint force resembles the load variation in the displacement-controlled case since the total deformation in the member is also imposed. When shrinkage strain develops, tensile stress-dependent strain also develops to maintain a constant length of the concrete member (black line in Fig. 2.5 (a)). Tensile stresses develop until they reach the tensile strength of the concrete (blue line in Fig. 2.5(a)). At that point, a crack forms and the restraint load drops so that the total deformation is kept unchanged, resulting in a reduction of the overall stiffness. For subsequent cracks to form, the restraint

force, which develops according to the new reduced stiffness, must rise again to a value slightly above the initial cracking load, meaning shrinkage strain needs to continue developing. It should be noted that, due to the fact that shrinkage develops slowly, creep and relaxation effects also occur, resulting in a gradual loss of stiffness and tensile stress (see red line in Fig. 2.5(a)) during the development of the restraint force. For restrained shrinkage, cracking will cease when the final shrinkage strain is attained, independently of whether the stabilized cracking stage has been reached.

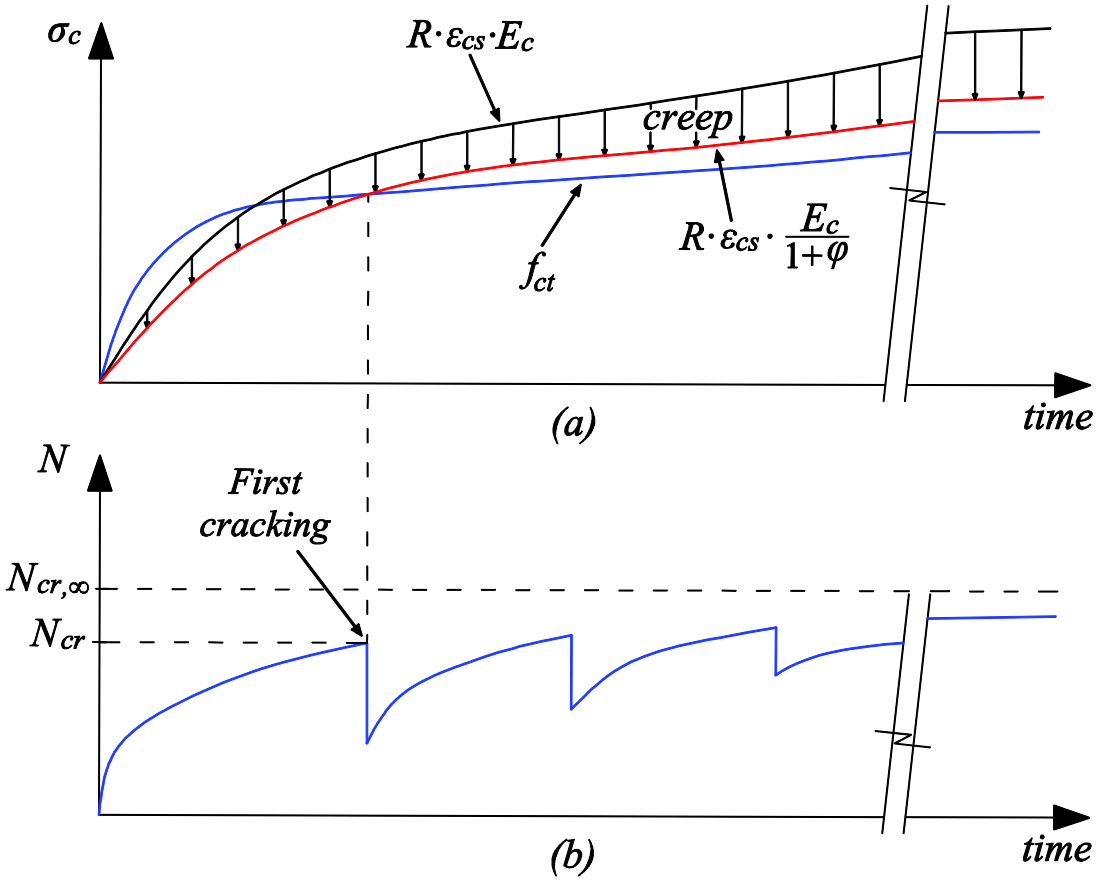

Figure 2.5. (a) Development of tensile strength of concrete as a function of time and evolution of the tensile stress due to restrained shrinkage strain, including creep effects, adapted from [11] *and (b) Restraint force history in a reinforced concrete member subjected to tensile loads due to restrained shrinkage strain, adapted from* [8].

2.2. Fibre reinforced concrete and hybrid reinforced concrete members

- *Fibre reinforced concrete*

Fibre reinforced concrete (FRC) is a cement-based composite material reinforced with short, discontinuous fibres dispersed throughout the concrete matrix. The main purpose behind adding fibres to concrete is to better control the fracture process by bridging discrete cracks. As a result, the presence of fibres increases the fracture energy of concrete, enhancing its toughness and leading to a more ductile behaviour. However, the post-cracking behaviour of FRC largely depends on various parameters, including the physical properties of the fibres, the fibre-matrix bond and the amount, orientation and distribution of the fibres throughout the concrete matrix [12].

Although fibres improve the toughness of the concrete in compression, the greatest beneficial effect of fibres is observed on the tensile properties. Accordingly, fibre reinforced cementitious materials may be classified based on their tensile behaviour, as either strain softening (a quasi-brittle material) or pseudo-strain hardening [13]. Plain concrete is a strain softening material characterized by a sudden loss of stress once the tensile strength of the material has been reached. Conversely, cementitious materials presenting pseudo-strain hardening behaviour exhibit multiple-cracking up to the post-cracking strength, which is higher than the cracking strength. In practice, it is generally accepted that low fibre contents, below 1% vol., will lead to strain softening behaviour while pseudo-strain hardening is associated with higher fibre fractions, usually above 2% vol. Typical curves for various cementitious materials presenting different tensile behaviour are presented in Fig. 2.6.

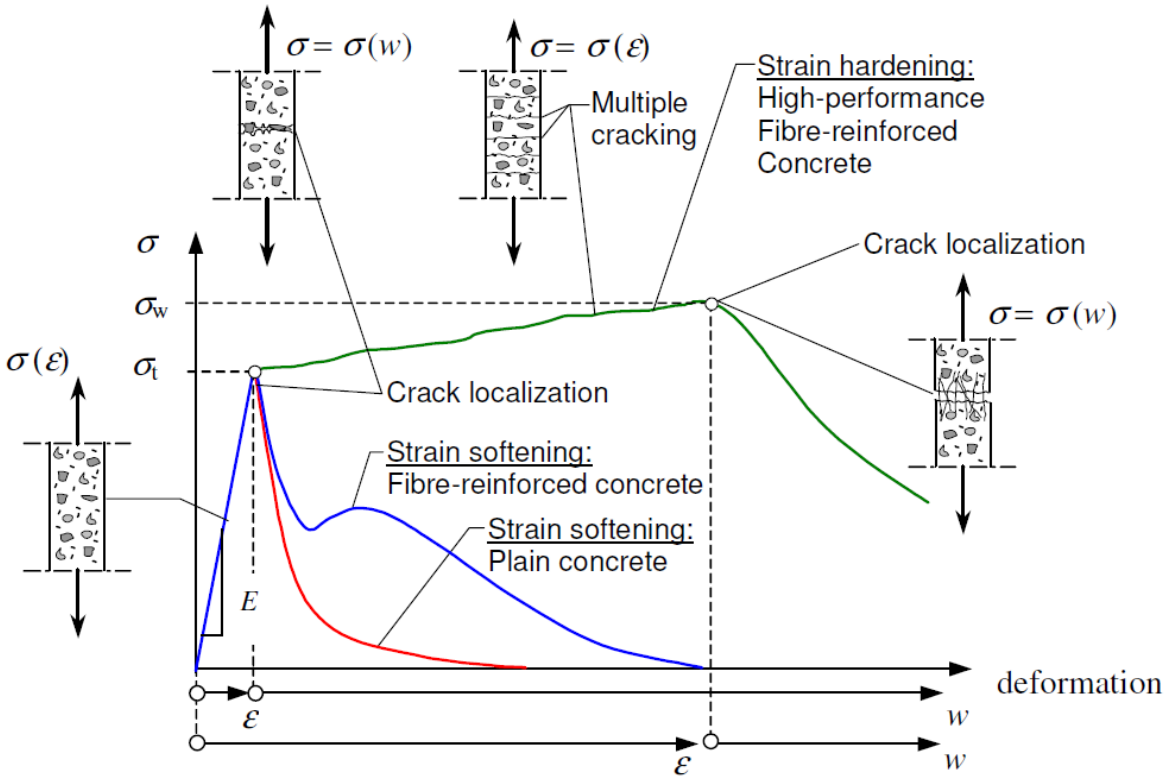

Figure 2.6. Tensile strength classification of cementitious materials, from [12]

FRC has been successfully employed to replace conventional reinforcement, either partially or entirely, in different structural applications and with different purposes, such as: in industrial floors and slabs on grade to arrest cracking, mostly due to plastic and drying shrinkage [12]; in tunnels as sprayed concrete [14] or precast segmental linings [15] to increase efficiency and reduce costs compared to conventional reinforcement systems; to improve the water tightness in containment structures [2]; and in thin shells or complex shape structures where conventional rebar systems are not suitable [16]. Several research studies have shown that fibre reinforcement is also particularly suitable for various structural applications, e.g. as shear reinforcement, see e.g. [17] or in seismic applications [18], where fibres have been regarded as having a similar or even better performance than conventional rebar.

However, according to Bentur and Mindess [19], it is unlikely that fibres will completely replace conventional reinforcement in large structural members. This can be attributed to the need for high fibre volume fractions and relatively high-performance concretes in order to obtain a pseudo-strain hardening behaviour, added to the low efficiency of fibres caused by their random position and orientation throughout the concrete matrix.

- *Hybrid reinforced concrete members*

Although fibre reinforcement may not be able to completely replace steel bars, a combination of both types of reinforcement, sometimes referred to as hybrid reinforcement, could be used to improve the mechanical response of RC elements [20]. Fibres can influence the behaviour of conventionally RC elements by carrying a fraction of the tensile load through cracks and by controlling the development of bond-splitting cracks. These two mechanisms lead to a series of enhancements, such as greater load-carrying capacity [21], increased tension-stiffening [22] and improved bond between the matrix and the bars due to the passive confinement provided by the fibres [23]. Nevertheless, one of the main advantages of using FRC in conventionally reinforced concrete elements is a better control of the cracking process, which results in a reduction of the crack widths and crack spacing [24–27]. Moreover, fibre reinforcement has been also found to reduce the interfacial damage occurring during mechanical loading between ribbed bars and the concrete matrix [28,29]. , which can be party attributed to an increase of the internal crack branching in hybrid reinforced members [30,31], see Fig. 2.7.

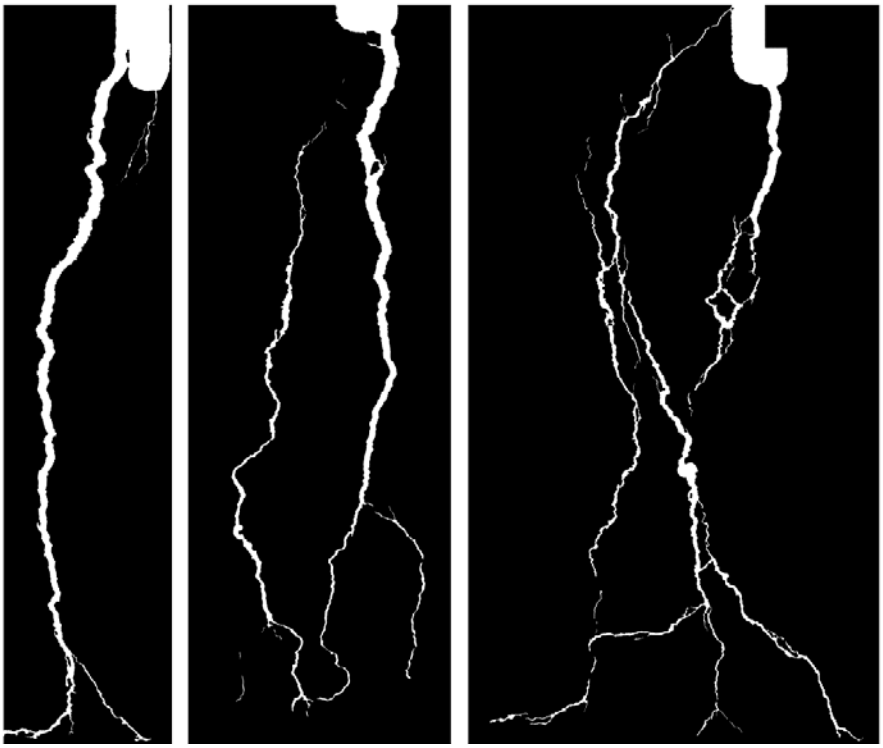

(a) (b) (c)

Figure 2.7. Internal crack profiles of beams subjected to bending for (a) reinforced concrete, (b) hybrid reinforced concrete with steel fibres only and (c) hybrid reinforced concrete with multi-scale fibre reinforcement (steel macro-fibres + PVA micro-fibres).

Consequently, combining fibre reinforcement and conventional steel bars could be beneficial with regard to various aspects. Due to the improved mechanical performance of RC elements made of fibre reinforced concrete compared to plain concrete, material savings could be achieved, e.g. by reducing the cover depths. Additionally, partially replacing conventional steel bars by fibre reinforcement would increase efficiency during the construction process and ameliorate the congested reinforcement layouts that are often incurred in structures exposed to harsh environments, thereby facilitating the casting procedure. Furthermore, fibres could be used for crack control purposes in order to mitigate the ingress of deleterious substances into the concrete and thus improve the overall durability of RC structures [32]. A successful application of hybrid reinforcement has been carried out by the Norwegian Public Roads Administration, Statens Vegvesen, where they used different types of fibre combined with conventional reinforcement to replace the edge beams of an existing bridge [33].

3. Calculation of crack width in RC structures

3.1. Crack width calculation due to load-induced cracking

- *Conventionally reinforced concrete*

As previously mentioned in Section 2.1, most expressions included in current codes and recommendations to calculate the crack width in reinforced concrete members are based on the study of a thin prismatic concrete specimen reinforced with a single centric bar subjected to uniaxial tension. The common way to calculate the crack width is by considering the compatibility of a segment between two consecutive cracks in a RC tie-element that has reached the stabilized cracking stage, according to:

$$w_k = s_{r,max}\,(\varepsilon_{sm} - \varepsilon_{cm}) \tag{3.1}$$

where ε_{sm} and ε_{cm} are the mean steel and concrete strains, respectively, and $s_{r,max}$ is the maximum crack separation equal to two times the transmission length, $s_{r,max} = 2 \cdot l_{t,max}$. The value of the transmission length can be derived by considering the equilibrium of forces in the segment between two consecutive cracks separated by the maximum crack distance, see Fig. 3.1.

When the RC tie element in Fig. 3.1 is subjected to a uniaxial tensile force equal to the crack load, N_{cr}, the stress in the concrete is assumed to be zero at the crack whereas at the midpoint between the two cracks, the concrete stress approaches the tensile strength, i.e. $\sigma_c \approx f_{ctm}$. The increase of stress in the concrete segment is a result of the stress transfer from the reinforcement to the concrete through bond. The bond stress, τ_b, varies along the transmission length and its average value τ_{bm} can be calculated as:

$$\tau_{bm} = \frac{\int_0^{l_{t,max}} \tau_b(x)dx}{l_{t,max}} \tag{3.2}$$

The equilibrium condition, for the concrete part only, between a crack and the middle section can be formulated as follows:

$$\pi \emptyset_b \tau_{bm} \cdot l_{t,max} = A_c \cdot f_{ctm} \tag{3.3}$$

where A_c is the concrete net area and $\emptyset_b$ is the reinforcement bar diameter. The concrete net area can be rewritten as:

$$A_c = A_s \cdot \frac{A_c}{A_s} = \frac{A_s}{\rho_s} = \frac{\emptyset_b^2 \pi}{4\rho_s} \tag{3.4}$$

with $\rho_s=A_s/A_c$ the reinforcement ratio. By replacing Eq. 3.4 into Eq. 3.3 and re-arranging the terms, the expression for the maximum transmission length, which in turn is the minimum crack spacing, can be obtained:

$$l_{t,max} = s_{r,min} = \frac{1}{4} \cdot \frac{f_{ctm}}{\tau_{bm}} \cdot \frac{\emptyset_b}{\rho_s} \tag{3.5}$$

Consequently, the maximum crack spacing, $s_{r,max} = 2 \cdot l_{t,max}$, can be expressed as:

$$s_{r,max} = \frac{1}{2} \cdot \frac{f_{ctm}}{\tau_{bm}} \cdot \frac{\emptyset_b}{\rho_s} \tag{3.6}$$

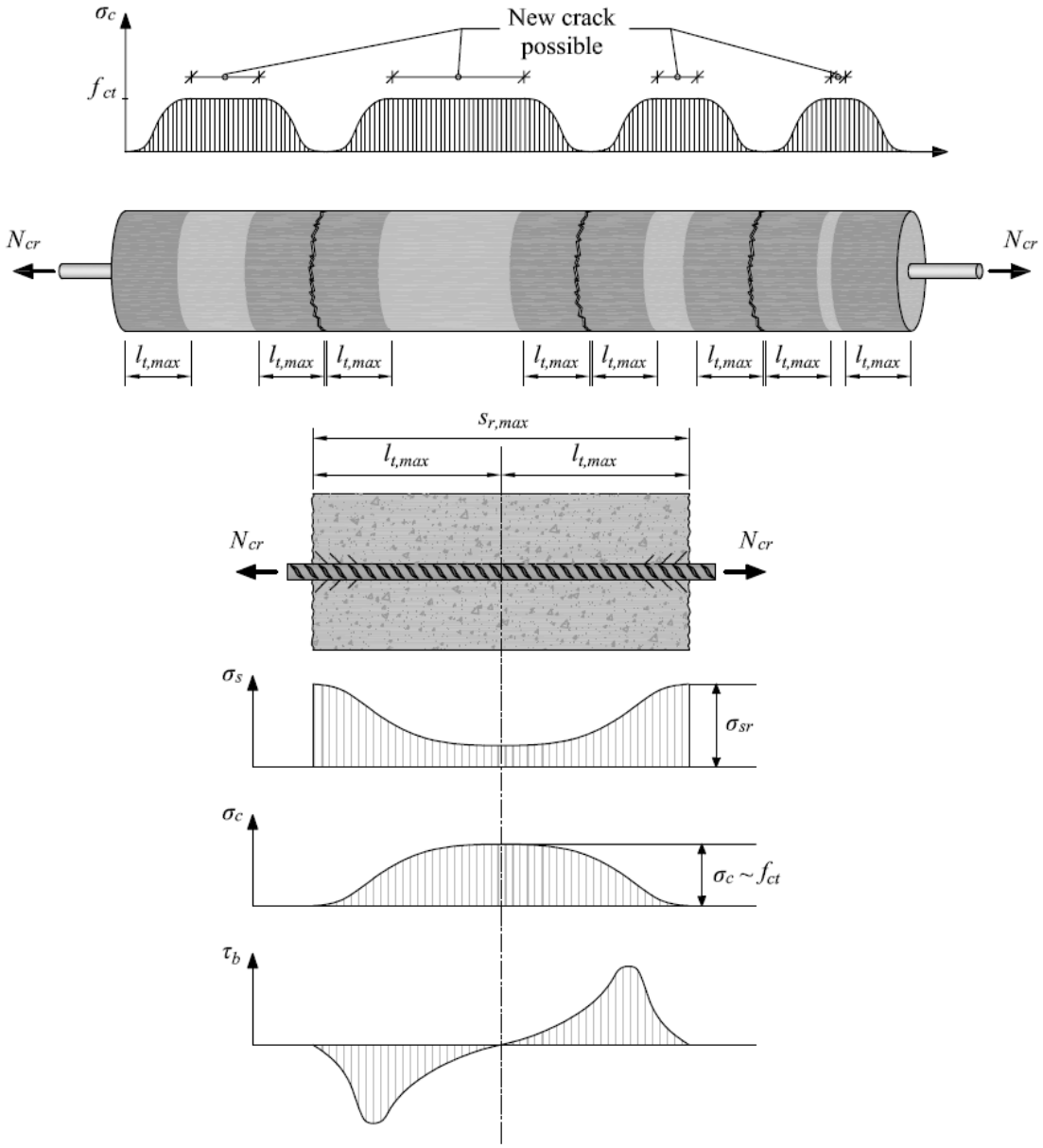

Figure 3.1 Prismatic concrete specimen with a single centric reinforcement bar subjected to uniaxial tension and the distribution of normal tensile stresses in the steel and concrete as well as bond stresses along a segment between two consecutive cracks of length equal to the maximum crack separation.

Eurocode 2

In the Eurocode 2 [34], the characteristic crack width to be compared with the maximum allowed crack width is calculated according to the expression previously shown in Eq. 3.1:

$$w_k = s_{r,max}\,(\varepsilon_{sm} - \varepsilon_{cm}) \tag{3.1}$$

where the term (ε_{sm} - ε_{cm}) is calculated as:

$$\varepsilon_{sm} - \varepsilon_{cm} = \frac{\sigma_s - k_t \frac{f_{ct}}{\rho_s}(1 + \alpha_e \rho_s)}{E_s} \geq 0.6\frac{\sigma_s}{E_s} \tag{3.7}$$

where σ_s is the stress in the tension reinforcement assuming a cracked section, $\alpha_e = E_s/E_c$ is the modular ratio, $\rho_s = A_s/A_c$ is the (tensile) reinforcement ratio and k_t is a factor dependent on the load duration equal to 0.6 for short-term loading and 0.4 for long-term loading. In the Eurocode 2, the maximum crack spacing is assumed to be 1.7 times the average crack spacing, s_{rm}, which can be calculated from Eq. 3.5 and Eq. 3.6 as:

$$s_{rm} = \frac{3}{8} \cdot \frac{f_{ctm}}{\tau_{bm}} \cdot \frac{\emptyset_b}{\rho_s} \tag{3.8}$$

Based on experimental results, it has been found that the average bond stress can be expressed in terms of the mean tensile strength of the concrete according to:

$$\tau_{bm} = \frac{3}{2 \cdot k_1} \cdot f_{ctm} \tag{3.9}$$

where k_1 is a factor taking into account the type of reinforcement and adopting a value of 0.8 for ribbed bars and 1.6 for smooth bars. By replacing Eq. 3.9 into Eq. 3.8 and including the effect of the concrete cover, c, and a factor k_2 to account for the distribution of strains across the concrete section, the maximum crack spacing according to Eurocode 2 can be written as:

$$s_{r,max} = 1.7 \cdot \left(2c + k_1 k_2 0.25 \cdot \frac{\emptyset_b}{\rho_s}\right) \tag{3.10}$$

Model Code 2010

The Model Code 2010 [35] adopts a slightly modified version of Eq. 3.1 to define the calculation of the design crack width according to:

$$w_d = 2l_{t,max}\,(\varepsilon_{sm} - \varepsilon_{cm} - \varepsilon_{cs}) \tag{3.11}$$

where the newly introduced term ε_{cs} accounts for the strain of the concrete due to shrinkage. The relative mean strain between steel and concrete in a segment between two cracks (ε_{sm} - ε_{cm} - ε_{cs}) is calculated as:

$$\varepsilon_{sm} - \varepsilon_{cm} - \varepsilon_{cs} = \frac{\sigma_s - \beta \cdot \sigma_{sr}}{E_s} - \eta_r \cdot \varepsilon_{sh} \tag{3.12}$$

where σ_s and σ_{sr} are the steel stress in the stabilised and crack formation stage, respectively, $\beta = 0.6$, is an empirical coefficient to assess the mean strain over the transmission length which depends on the type of loading and the product $\eta_r \cdot \varepsilon_{sh}$ accounts for the shrinkage strain contribution. On the other hand, the expression for the maximum transmission length is adopted as in Eq. 3.5 including the contribution of the concrete cover:

$$l_{t,max} = k \cdot c + \frac{1}{4} \cdot \frac{f_{ctm}}{\tau_{bm}} \cdot \frac{\emptyset_b}{\rho_s} \tag{3.13}$$

where k is by simplicity assumed to be equal to 1 and τ_{bm} is, for most cases, taken as $1.8 \cdot f_{ctm}$.

ACI 224R-01

Unlike the Eurocode 2 and the Model Code 2010 which are based on a mechanistic model taking into account the transfer of bond stresses between the steel and concrete along the transmission length, the provisions given by the American Concrete Institute to calculate the crack width in reinforced concrete members subjected to flexural loads are based on an empirical model derived from the statistical analysis of crack-width data from a number of experimental tests. The equations considered in the ACI 224R-01 [11] are:

$$w_b = 0.091 \sqrt[3]{t_b A}\, \beta (f_s - 5) \cdot 10^{-3} \tag{3.14a}$$

$$w_s = \frac{0.091 \sqrt[3]{t_b A}}{1 + t_s / h_1} (f_s - 5) \cdot 10^{-3} \tag{3.14b}$$

where w_b and w_s are the crack width at the concrete surface and at the reinforcement level, respectively, f_s is the reinforcement steel stress, A is the area of concrete symmetric with reinforcing steel divided by number of bars, t_b and t_s are the bottom and side cover, respectively, h_1 is the distance from the neutral axis to the reinforcement and β is the distance from the neutral axis to the tension face divided by h_1.

- *Hybrid reinforced concrete*

Models based on modifications of the formulation provided in the Eurocode 2

In the final recommendation of RILEM TC 162-TDF [36], a semi-empirical method is proposed to calculate the crack width in reinforced concrete elements with fibre reinforcement, based on

a modification of the current formulation provided by the Eurocode 2 for elements without fibres. The model introduces a factor that accounts for the reduction in average crack spacing due to increasing aspect ratio of the fibres according to:

$$s_{rm} = \left(50 + \ 0.25 \cdot k_1 k_2 \cdot \frac{\emptyset_b}{\rho_s}\right)\left(\frac{50}{L_f/\emptyset_f}\right) \tag{3.15}$$

where L_f and $\emptyset_f$ are the fibre length and fibre diameter, respectively, and the rest of parameters remain unchanged. Furthermore, the following condition is imposed:

$$\left(\frac{50}{L_f/\emptyset_f}\right) \leq 1 \tag{3.16}$$

which means that only the fibres with an aspect ratio greater than 50 will result in a reduction of the average crack spacing, hence of the mean crack width.

Analogously as for the model proposed by the RILEM TC 162-TDF, an alternative modification of the average crack spacing based on the formulation provided by the Eurocode 2 has been suggested by Moffatt [37] and Löfgren [4]. In this case, an additional factor is added to the second term of Eq. 3.10 which reduces the average crack spacing based on the ratio of the post-cracking residual stress of FRC to the tensile strength of the concrete according to:

$$s_{rm} = 50 + \ 0.25 \cdot k_1 k_2 \cdot \frac{\emptyset_b}{\rho_s}\left(1 - \frac{f_{res}}{f_{ct}}\right) \tag{3.17a}$$

where f_{res} and f_{ct} are the post-cracking residual stress and the tensile strength of the concrete, respectively. It should be noted that the expression given by Eq. 3.17a is only applicable to fibre reinforced concrete exhibiting strain-softening behaviour.

An alternative expression, similar to the one proposed by Moffatt and by Löfgren, was suggested in a master's thesis by Gustafsson and Karlsson [38] , which in addition to the newly added term, considers the effect of the concrete cover and bar diameter on the crack spacing according to:

$$s_{rm} = c + 3 \cdot \emptyset_b + \ 0.25 \cdot k_1 k_2 \cdot \frac{\emptyset_b}{\rho_s}\left(1 - \frac{f_{res}}{f_{ct}}\right) \tag{3.17b}$$

where c is the thickness of the concrete cover.

Model by Deluce et al.

Another model to calculate the crack width in hybrid reinforced concrete elements was proposed by Deluce et al. [39]. The model formulation is based on the stabilized crack spacing

formulation given by the CEB-FIP Model Code 1978 [40], introducing new parameters that account for the fibre content, length and diameter, according to:

$$s_m = 2\left(c_a + \frac{s_b}{10}\right)k_3 + \frac{k_1 k_2}{s_{mi}} \tag{3.18}$$

where k_1 and k_2 have the same meaning as in Eq. 3.15, the factor k_3 is introduced to account for the beneficial effect of fibres in relation to the cover, c_a, and bar spacing, s_b, whereas the reinforcement effectiveness parameter s_{mi} is also modified to take into consideration the tensile stress attained by bridging fibres at the crack as:

$$s_{mi} = \frac{\rho_s}{\emptyset_b} + k_f \frac{\alpha_f V_f}{\emptyset_f} \tag{3.19}$$

where α_f is the orientation factor, which can be taken as 0.5 for 3D randomly oriented fibres, and V_f is the volume fraction, which is limited to 0.015 to account for the fact that above a certain dosage of about 1.5% vol. only a limited improvement in the tensile stress is observed. The parameter k_f is introduced to account for the effect of the aspect ratio as $k_f = L_f / 50\ \emptyset_f \geq 1$ in accordance to the RILEM TC 162-TDF formulation. The parameter k_3 can be calculated according to:

$$k_3 = 1 - \frac{\min(V_f, 0.015)}{0.015}\left(1 - \frac{1}{k_f}\right) \tag{3.20}$$

Finally, due to the observed increase in the ratio between the maximum and average crack width in FRC members with respect to plain concrete ones, a new expression was also proposed to calculate the maximum crack width from the average crack width as:

$$w_{max} = \left(1.7 + 3.4\frac{V_f L_f}{\emptyset_f}\right) w_{avg} \tag{3.21}$$

3.2. Control of restraint cracking and available calculation models

When cracking is caused by external loading, a minimum reinforcement is commonly designed to ensure that the total load carried out by the effective area of concrete in tension before cracking can be carried by the reinforcement alone without yielding. In the stabilized cracking stage, the width of the formed cracks can be controlled, e.g. by limiting the stress at the reinforcement.

In restrained concrete members subjected to shrinkage or thermal contraction, the design of minimum reinforcement and crack width calculations cannot be performed in the same manner as in members subjected to direct loading since the restraint force, which depends on the stiffness of the member, is not known a priori. As the overall stiffness of the member decreases

whenever a new crack forms, the restraint force decreases accordingly to adapt to the imposed deformation. Nevertheless, controlling restraint cracking is equally important in order to avoid excessively large crack widths. As previously mentioned, crack formation might stop before the stabilised cracking stage is reached and, in the worst case, the restraint force might decrease so much after the formation of the first crack that subsequent cracks could be unable to form thereby concentrating all the deformation in a single opening crack.

Some of the existing methodologies and models from the literature dealing with control of shrinkage cracking and restraint cracking analysis are presented and briefly discussed in the following.

- *ACI 224R-01*

The ACI 224R-01 report titled "Control of Cracking in Concrete Structures" by the American Concrete Institute [11], describes the phenomena of concrete shrinkage strain and restraint cracking but it does not contain specific provisions to calculate or limit the crack width of concrete elements subjected to restraint cracking. Instead, a very general recommendation is given to provide sufficient reinforcement to achieve reinforcement ratios exceeding 0.6%, i.e. $\rho=A_s/A_c$ >0.006, as described in the following paragraph, literally extracted from the report:

> *"The minimum amount and spacing of reinforcement to be used in structural floors, roof slabs, and walls for control of temperature and shrinkage cracking is given in ACI 318 or in ACI 350R. The minimum-reinforcement percentage, which is between 0.18 and 0.20%, does not normally control cracks to within generally acceptable design limits. To control cracks to a more acceptable level, the percentage requirement needs to exceed about 0.60%."*

- *Eurocode 2 and Model Code 2010*

In the current version of the Eurocode 2 [34] and Model Code 2010 [35], the control of cracking is treated without direct calculations when the main cause is restraint. The provisions included in the Eurocode 2 and Model Code 2010 state that crack widths will not exceed a certain threshold provided the diameter of the reinforcement bars used is limited based on the steel stress obtained in the reinforcement immediately after cracking, according to Table 3.1:

Table 3.1. Maximum bar diameters for crack control according to Eurocode 2 [34].

Steel stress [MPa]	Maximum bar size [mm]		
	w_k = 0.4 mm	w_k = 0.3 mm	w_k = 0.2 mm
160	40	32	25
200	32	25	16
240	25	16	12
280	16	12	8
320	12	10	6
360	10	8	5
400	8	6	4
450	6	5	-

The steel stress can be calculated according to Eq. (3.22):

$$\sigma_s = k_c k\, f_{ct,ef}\, A_{ct}/A_s \tag{3.22}$$

where A_{ct} is the area of concrete within the tensile zone, $f_{ct,ef}$ is the mean value of the tensile strength at the time when the first crack may occur, A_s is the area of reinforcing steel within the tensile zone and k and k_c are coefficients to account for the effect of non-uniform self-equilibrating stresses and the stress distribution within the section immediately prior to cracking, respectively.

- *BS 8007*

The approach provided in BS 8007 [41] for cracking due to restrained contraction caused by shrinkage or thermal strain is based on a simple bond-slip relationship, in which the transmission length, l_t, is expressed as a function of the bar diameter, Ø, the reinforcement ratio, $\rho=A_s/A_c$, the average tensile strength of the concrete, f_{ct}, and the average bond stress at the steel-concrete interface, τ_b, according to:

$$l_t = \frac{\emptyset}{4\rho}\frac{f_{ct}}{\tau_b} \tag{3.23}$$

where the average bond stress can be taken as $\tau_b = 2.4$ N/mm^2 for ribbed bars. The transmission length is regarded as the minimum crack spacing, $s_{r,min}$, whereas the maximum crack spacing $s_{r,max}$, corresponds to twice the transmission length, which can be expressed as:

$$s_{r,max} = 2l_t = \frac{\emptyset}{2\rho}\frac{f_{ct}}{\tau_b} \tag{3.24}$$

The maximum crack width can then be calculated based on the maximum crack spacing and the effective strain, according to:

$$w_{max} = s_{r,max}\, \varepsilon \tag{3.25}$$

where the effective strain ε accounts for the total strain arising from concrete shrinkage and thermal contraction minus a constant deducted strain of $100 \cdot 10^{-6}$.

- *Model by Nejadi and Gilbert*

In the model by Nejadi and Gilbert [42], the authors first analyse the case of a single crack in a fully-restrained direct tension member. Immediately after the first crack occurs, the concrete stress at the crack becomes zero and the concrete shortens elastically giving rise to a certain crack width, w. Through bond action, stress transfer develops over a certain transmission length, l_t, assuming a parabolic stress variation. Accordingly, the concrete stress varies from zero at the crack to a certain tensile stress, σ_{c1}, at a distance l_t from the crack. Conversely, the steel carries the entire restraint force at the crack resulting in a tensile stress, σ_{s2}, which decreases to a

compressive stress, σ_{s1}, at a distance l_t from the crack. Nejadi and Gilbert assumed a constant value of the transmission length equal to:

$$l_t = \emptyset/(10\rho) \tag{3.26}$$

where $\emptyset$ is the bar diameter and $\rho=A_s/A_c$ is the reinforcement ratio. However, Nejadi and Gilbert noted that the value of l_t should be increased to $\emptyset/(7.5\,\rho)$ for long-term calculations or at a final stage due to a gradual deterioration of the bond at the steel-concrete interface with time.

After first cracking, the concrete stress, σ_{c1}, at a distance l_t from the crack and the steel stress at the crack σ_{s2}, are given by the following expressions:

$$\sigma_{c1} = \frac{3L \cdot \alpha\rho f_{ct}}{2l_t + 3L \cdot \alpha\rho} \tag{3.27}$$

$$\sigma_{s2} = \frac{(3L - 2l_t) \cdot \alpha f_{ct}}{2l_t + 3L \cdot \alpha\rho} \tag{3.28}$$

where L is the total length of the member between restraints, f_{ct} is the concrete tensile strength and $\alpha = E_s/E_c$ is the modular ratio. For a more general case in which the restraints at the end of the member are only partial, and assuming that all the shrinkage has taken place, the crack formation phase is ended and creep effects are accounted for, the final concrete stress, σ_{c1}^{∞}, at a distance l_t from the crack and the steel stress at the crack σ_{s2}^{∞}, are given by the following expressions:

$$\sigma_{c1}^{\infty} = \frac{3E_s\Delta u}{2n_{cr}l_t} - \frac{3L \cdot \alpha_{ef}\rho}{2n_{cr}l_t}\left(\sigma_{av} + \varepsilon_{cs}^{\infty}E_{c,ef}\right) \leq f_{ct} \tag{3.29}$$

$$\sigma_{s2}^{\infty} = \frac{3E_s\Delta u}{2n_{cr}l_t} - \frac{(3L - 2n_{Cr}l_t) \cdot \alpha_{ef}}{2n_{cr}l_t}(\sigma_{av} + \varepsilon_{cs}^{\infty}E_{c,ef}) \tag{3.30}$$

where Δu is the change in length of the member due to movement at the restraining supports, n_{cr} is the number of cracks, σ_{av} is the average stress of the concrete in the uncracked region, $\varepsilon_{cs}^{\infty}$ is the ultimate shrinkage strain, and $E_{c,ef}$ and $\alpha_{ef} = E_s/E_{c,ef}$ are the effective elastic modulus of the concrete and the effective modular ratio, respectively. In their calculations, Nejadi and Gilbert assume a value of the average concrete stress equal to $\sigma_{av} = (\sigma_{c1} + f_{ct})/2$, whereas the effective modulus may be taken as $E_{c,ef} = 1/(1+\varphi)$, where φ is the final creep coefficient. The number of cracks n_{cr} is taken as the minimum integer so that the condition $\sigma_{c1}^{\infty} \leq f_{ct}$ is fulfilled. Finally, assuming that steel reinforcement does not yield after cracking, the following expression for the average crack width is obtained:

$$w = -\left[\frac{\sigma_{c1}^{\infty}}{E_{c,ef}}\left(\frac{L}{n_{cr}} - \frac{2}{3}l_t\right) + \varepsilon_{cs}^{\infty}\left(\frac{L}{n_{cr}}\right)\right] \tag{3.31}$$

- *Häußler-Combe and Hartig*

The approach followed by Häußler-Combe and Hartig [43] also departs from the idea of a reinforced concrete member subjected to direct tension in which a symmetric crack exists with adjacent bond transfer regions of equal transmission length. The concrete stress is assumed to vary from zero at the crack location to a maximum value at the end of the transmission length whereas the stress at the reinforcement is maximum at the crack and decreases to a minimum value at the end of the transmission length. Accordingly, the average crack width w in the member can be expressed in terms of the transmission length l_t and the mean strains in the steel ε_{sm} and in the concrete ε_{cm} as:

$$w = 2l_t(\varepsilon_{sm} - \varepsilon_{cm}) \tag{3.32}$$

The mean strains can be calculated from the corresponding mean stresses, σ_{sm} and σ_{cm} which can be expressed in terms of the maximum stress of the reinforcement at the crack σ_{sr} and the total variation of stresses in the steel $\Delta\sigma_s$ as:

$$\sigma_{sm} = \sigma_{sr} - \beta_t \Delta\sigma_s \tag{3.33}$$

$$\sigma_{cm} = \rho\beta_t \Delta\sigma_s \tag{3.34}$$

where $\rho=A_s/A_c$ is the reinforcement ratio and β_t is an empirical factor describing the shape of the stress distribution in the steel along the transmission length, which can be assumed to adopt a constant value of 0.4 for long-term imposed loading. Based on the force equilibrium between the normal stresses in the steel and the bond stresses acting at the steel-concrete interface along the transmission length, the following expression for variation in the steel stress is attained:

$$\Delta\sigma_s = \frac{4l_t}{\emptyset}\,\tau_{bm} \tag{3.35}$$

where τ_{bm} is the mean bond stress, which can be assumed to be proportional to the tensile strength of the concrete according to:

$$\tau_{bm} = \gamma f_{ct} \tag{3.36}$$

where the value of gamma is commonly taken as 1.8 for most loading situations. In the stabilized cracking phase, the stress in the concrete is necessarily lower than the cracking strength f_{ct} since no new cracks can be formed. Since the stress in the concrete varies from zero at the crack to a maximum value of $\rho\Delta\sigma_s$ at the end of the transmission length, $\Delta\sigma_s$ needs to be smaller than f_{ct}/ρ. By replacing the value of $\Delta\sigma_s = f_{ct}/\rho$ in Eq. 3.35, an upper limit of the transmission length $l_{t,max}$ can be found:

$$l_{t,max} = \frac{\emptyset}{4\rho}\frac{f_{ct}}{\tau_{bm}} \tag{3.37}$$

From Eq. 3.37 it follows that if the separation between two cracks is equal or greater than twice the maximum transmission length, a new crack can form between the existing cracks. Conversely, the minimum possible distance between two consecutive cracks is the distance required to reach the tensile strength in the concrete, i.e. maximum transmission length. Therefore, the crack spacing s_r must fulfil the following condition:

$$l_{t,max} \leq s_r \leq 2l_{t,max} \tag{3.38}$$

For a reinforced concrete member subjected to an imposed strain $\varepsilon_{cE}<0$ which is uniformly distributed along its entire length L, and a certain number of cracks n_{cr} the imposition of the compatibility condition yields the following expression:

$$w = -\frac{1}{n_{cr}}\left[L\varepsilon_{cE} + \frac{1}{E_c}\int_L \sigma_c(x)dx - \Delta u\right] \tag{3.39}$$

where Δu is the change in length of the member due to support movement. Häuβler-Combe and Hartig distinguished between two cases, crack formation phase and stabilised cracking phase. In the former case, new cracks can be formed and therefore the total length of the member can be divided between the regions adjacent to the cracks where the concrete stress varies and regions beyond the transmission length where the concrete stress is constant. In the stabilised cracking phases, since no new cracks can be formed, the entire length of the member consists of transmission lengths and therefore the concrete stress varies along the entire length. Consequently, Eq. 3.39 leads to two different expressions depending on the following condition:

$2n_{cr}l_t < L \quad \rightarrow$ Crack formation phase (3.40a)

$2n_{cr}l_t \geq L \quad \rightarrow$ Stabilised cracking phases (3.40b)

For the crack formation phase, the crack width can be calculated according to:

$$w = \frac{\emptyset}{2\tau_{bm}}\frac{(1+\alpha_e\rho)(1-\beta_t)}{E_S}\,\Delta\sigma_S^2 \tag{3.41}$$

where $\Delta\sigma_s$ can be calculated as:

$$\Delta\sigma_S = \sqrt{\left(\frac{1}{2}\frac{\bar{t}L}{n_{Cr}}\alpha_e\rho\right)^2 - \frac{\bar{t}E_s}{n_{Cr}}(L\varepsilon_{cE} - \Delta u)} - \frac{1}{2}\frac{\bar{t}L}{n_{Cr}}\alpha_e\rho\,; \quad \bar{t} = \frac{2\tau_{bm}}{\emptyset(1-\beta_t)} \tag{3.42}$$

On the other hand, for the stabilized cracking phase, the expression of the crack width becomes:

$$w = \frac{\emptyset f_{ct}}{2\tau_{bm}\rho}\left(\varepsilon_{cE} + \beta_t \frac{f_{Ct}}{E_{c,ef}} - \frac{\Delta u}{L}\right) \tag{3.43}$$

In Eq. 3.41 and Eq. 3.43 the effective elastic modulus of the concrete $E_{c,ef}$ and the corresponding effective modular ratio $\alpha_{ef} = E_s/E_{c,ef}$ are used to account for creep effects. The effective elastic modulus of the concrete can be calculated as $E_{c,ef} = 1/(1+\varphi)$, where φ is the final creep coefficient.

3.3. Proposed model for crack width calculation in R/FRC due to restraint cracking

It is apparent that while some structural design codes do not provide tools to calculate the crack width due to restraint cracking and they limit the design approach to provide a minimum reinforcement amount, others employ models developed for load-induced cracking that assume stabilized cracking stage, which is often not the case. On the other hand, the main shortcoming of the restraint cracking models presented in the previous section is that they do not take into consideration the bond characteristics of the embedded reinforcement, hence the calculated transmission length and crack width are not dependent on the shape of the bond-slip relationship. The restraint cracking model presented in this section is a modification of a model originally developed by Engström [3], which is derived assuming a realistic non-linear bond-slip relationship suggested by a joint CEB-FIP Working Group [44] as an extension of the model provided in the fib Model Code 1990 [45] for crack width calculations in serviceability limit state. The main idea behind the model proposed by Engström is that restraint cracking can be analysed assuming that cracks behave as non-linear springs, see Fig. 3.2.

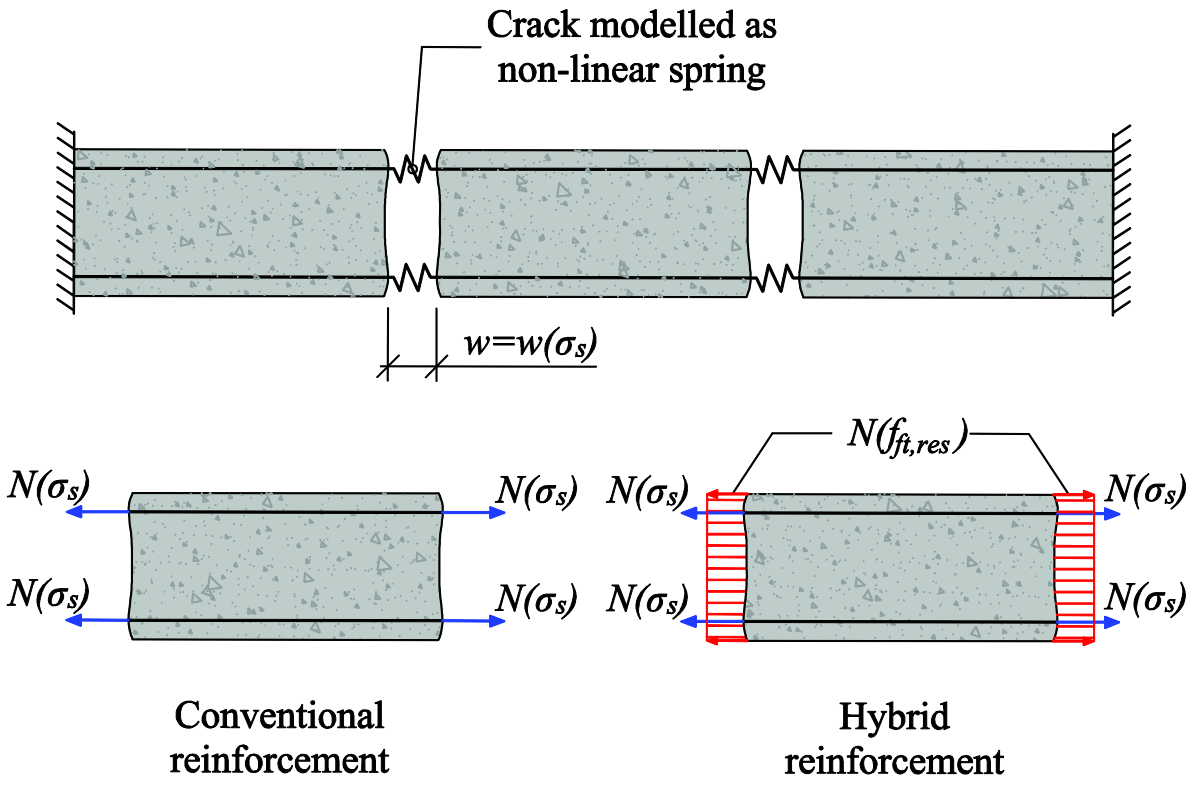

Figure 3.2 Schematic drawing illustrating the concept of the proposed model for analysing restraint cracking, after [4].

- *Original model by Engström*

The model is based on the study of the response of single cracks during the crack formation phase. At a cracked section, all the force is carried by the reinforcement whereas the concrete is assumed stress-free. Inside the concrete, a certain relative slip between the reinforcement and concrete occurs, which gives rise to the development of bond stresses within the transmission length. If the local relationship between bond stress and slip is known and can be mathematically formulated, the differential equation governing the equilibrium of normal and shear stresses in the reinforcement has an analytical solution provided certain regularity conditions of the bond-slip function are satisfied. For the particular case of bond-slip relationship in the form of power functions, $\tau(s) = \tau_{max} \cdot s^{\alpha}$ with $0<\alpha<1$, it can be demonstrated that an analytical solution exists for the case of single cracks [46]. In CEB 228 [44], an empirical bond-slip relationship is formulated, where the initial branch, which is the relevant part for service state conditions, corresponds to the following power function:

$$\tau_b(s) = 0.22\, f_{cm} \cdot s^{0.21} \tag{3.44}$$

where f_{cm} is the average compressive strength of the concrete and s is the slip along the transmission length. Using Eq. 3.44 as a basis, Engström derived expressions for the transmission length, Eq. 3.45, and the corresponding mean crack width, Eq. 3.46, as a function of the steel stress at the cracked section:

$$l_t(\sigma_s) = 0.443 \frac{\emptyset \cdot \sigma_S}{0.22 f_{cm} w_{net}^{0.21} \left(1 + \alpha_{ef}\rho\right)} + 2\emptyset \tag{3.45}$$

$$w(\sigma_s) = 0.42 \left(\frac{\emptyset \sigma_s^2}{0.22 f_{cm} E_s \left(1 + \alpha_{ef}\rho\right)}\right)^{0.826} + 4\emptyset \frac{\sigma_S}{E_s} \tag{3.46}$$

where $\emptyset$ is the bar diameter, σ_s is the stress in the reinforcement at the crack, $\rho = A_s/A_c$ is the reinforcement ratio, being A_c the effective concrete area in the tensile zone and $\alpha_{ef} = E_s/E_{c,ef}$ is the effective modular ratio, in which $E_{c,ef} = 1/(1+\varphi)$ is the effective elastic modulus of concrete including the creep effects, being φ the final creep coefficient. The net crack width, w_{net}, in Eq. 3.45 corresponds to the first term on the right-hand side in Eq. 3.46, whereas the second term on the both expressions above corresponds to a certain length adjacent to the crack where bond is assumed to be fully broken due to radial cracking towards the free surface.

The cracking response of a concrete element subjected to restrained shrinkage or thermal contraction can be described using the following deformation compatibility condition:

$$\frac{N(\sigma_s)}{E_{ef} A_I} l + n_{cr} \cdot w(\sigma_s) + R \cdot \varepsilon_{cs} \cdot l = 0 \tag{3.47}$$

where $N(\sigma_s) = A_s \cdot \sigma_s$ is the axial force acting on the uncracked parts of the element (see Fig. 3.2), l is the total length of the element, $A_I = A_c + A_s(E_s/E_c - 1)$ is the area of the transformed concrete section, n_{cr} is the number of cracks, ε_{cs} is the final shrinkage (or thermal contraction) strain and R is the degree of restraint ($R = 1$ for full restraint and for $R = 0$ for free movement). The first term in Eq. 3.47 represents the elongation of the uncracked parts in the element whereas the second term accounts for accumulated deformation due to crack opening which can be described by the expression given in Eq. 3.46. The last term takes into consideration an eventual displacement of the supports.

The general approach of the model follows an iterative procedure in which the model is initiated for $n_{cr} = 1$, and then the value of $N(\sigma_s)$ is calculated from Eq. 3.47. If $N(\sigma_s)$ is smaller than the force required to initiate a new crack, N_{cr}, only one crack will be formed, whereas if it is greater, more cracks can be formed. Then, the number of cracks is increased according to $n_{cr} = n_{cr} + 1$ and the process is successively repeated until the cracking process is stopped, either because the build-up force is not enough to form a new crack, $N(\sigma_s) < N_{cr}$, or because the average crack spacing has decreased to its minimum possible value, $l/(n_{cr}+1) < l_{t,max}$. The force required to initiate a new crack can be expressed as:

$$N_{cr} = f_{ctm} \left(A_c + \left(\frac{E_S}{E_c} - 1\right) A_s\right) \tag{3.48}$$

where f_{ctm} is the average tensile strength of the concrete. When the number of cracks is known, the actual crack width can be calculated from Eq. 3.46. Since Eq. 3.46 is a non-linear

expression, finding the value of σ_s that fulfils the compatibility condition expressed by Eq. 3.47 is not straightforward. However, the expression of the crack width as a function of the steel stress in the second term of Eq. 3.47 can be conservatively replaced by a linear approximation according to:

$$w(\sigma_s) \cong \frac{w(f_y)}{f_y}\,\sigma_s \tag{3.49}$$

where f_y is the yield stress of the steel reinforcement.

- *Modified Engström's model*

Three main modifications have been introduced with respect to the original model by Engström [3]. The first modification is a change of the expression used to define the bond-slip relationship, which has been replaced by the one suggested in the new Model Code 2010 [35]:

$$\tau_b(s) = 2.5\sqrt{f_{cm}} \cdot s^{0.4} \tag{3.50}$$

As observed in Fig. 3.3, there are two main differences between the two expressions. The first difference is a slight reduction in the initial stiffness of the bond-slip relationship while the second difference is a greater value of the maximum bond stress for the expression in the Model Code 2010. Even though both of these differences are dependent on the concrete strength, the former becomes more apparent as the concrete strength increases whereas the opposite occurs for the latter.

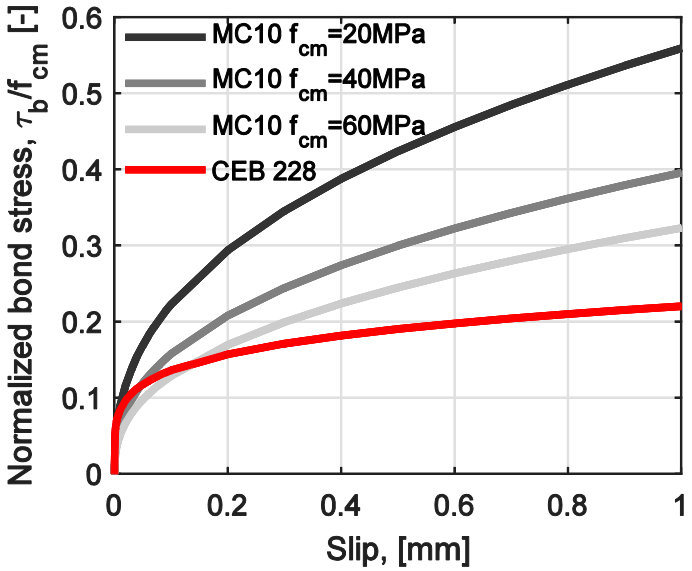

Figure 3.3. Normalized bon- slip relationships suggested in the CEB 228 [REF] and the Model Code 2010 [35] *for various concrete strengths.*

A decrease in the initial stiffness of the bond slip relationship could have a noticeable impact on the calculation of the crack width whereas an increase of the maximum bond stress is more relevant for ultimate limit state calculations. A comparison of the effect of the chosen bond-slip relationship on the (net) crack width calculation as a function of the steel stress is presented in Fig. 3.4 for two different concrete strengths. Based on the similarities between the two models

for the higher concrete strength, it seems that the relevant part of the bond-slip relationship for crack width calculation is the one describing slips of up to 0.2 mm. Furthermore, even if the bond stresses are significantly higher in the mentioned slip range, as for the lower strength concrete, the impact on the crack width is still limited and only apparent at relatively high steel stresses.

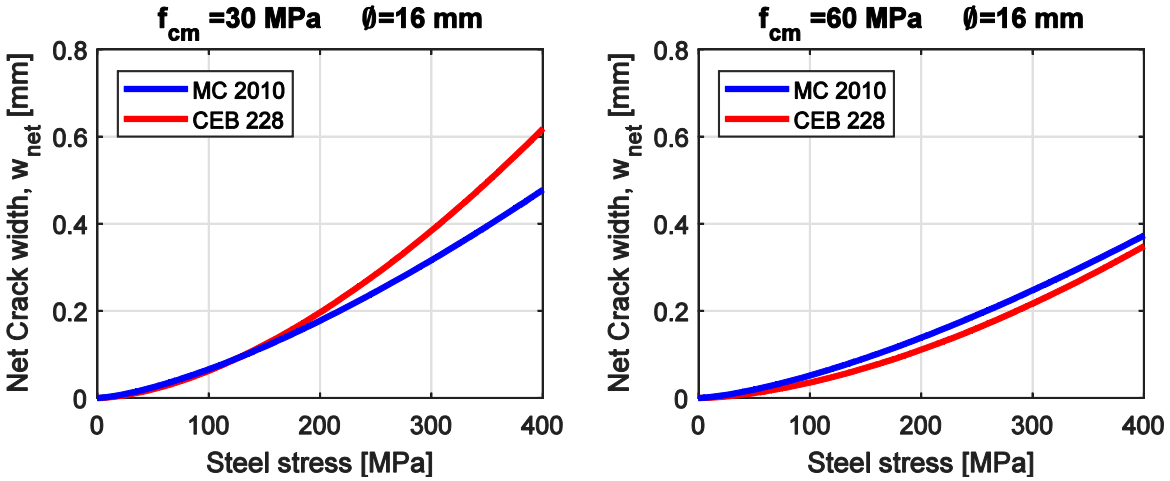

Figure 3.4. Effect of the bond-slip relationship on the (net) crack width calculation as a function of the stress at the reinforcement

The second change in the suggested model with respect to the original model by Engström is a modification of the second term in Eq. 3.45 and 3.46. As previously mentioned, that term corresponds to a certain length adjacent to the crack where bond is assumed to be fully broken due to radial cracking towards the free surface. Since the original model was developed to analyse ultimate limit states, that length is assumed constant. However, for service limit states is does not seem reasonable that the length along which the bond is fully broken reaches its maximum value as soon as any stress is applied on the reinforcement. Therefore, this term is modified to be linearly dependent on the stress level at the reinforcement, where the maximum length is assumed to be attained when steel reaches yielding. Moreover, in has been shown that bond degradation in fibre reinforced concrete is significantly reduced compared to plain concrete, even for large slips [47]. This is mainly due to the fact that fibres can arrest splitting cracks thereby keeping the confining effect of the concrete cover [28]. Accordingly, an additional factor is included in the second term of Eq. 3.45 and Eq. 3.46 to account for the beneficial effect of fibres, which is inversely proportional to the residual tensile strength of the fibre reinforced concrete.

Finally, the last change is a further development of the model, introduced by Löfgren [10], in order to include the effect of fibre reinforcement. This change is introduced in the model by modifying the first term of Eq. 3.47 to include the contribution of the fibres on the elongation of the uncracked parts the element, according to:

$$N(\sigma_s) = \sigma_s \cdot A_S + f_{fR1} \cdot A_c \tag{3.51}$$

With the corresponding changes, the new expressions for the transmission length Eq. 3.52 and the corresponding mean crack width Eq. 3.53 as a function of the steel stress at the cracked section can be rewritten as follows:

$$l_t(\sigma_s) = 0.77\frac{\emptyset \cdot \sigma_S}{2.5\sqrt{f_{cm}}w_{net}^{0.4}(1+\alpha_{ef}\rho)} + 2\emptyset\frac{\sigma_s}{f_y}\left(1-\frac{f_{ft,res}}{f_{ctm}}\right) \quad (3.52)$$

$$w(\sigma_s) = 0.576\left(\frac{\emptyset\sigma_s^2}{2.5\sqrt{f_{cm}}E_s(1+\alpha_{ef}\rho)}\right)^{0.714} + 4\emptyset\frac{\sigma_S^2}{E_s f_y}\left(1-\frac{f_{ft,res}}{f_{ctm}}\right) \quad (3.53)$$

It should be noted that the relationship between (net) crack width and steel stress is independent of the use of fibre reinforced concrete and its properties. Conversely, the beneficial effect of fibre reinforcement in reducing the crack width arises from the ability of fibres to retain the integrity of the concrete cover as well as decreasing the stress in conventional reinforcement according to Eq. 3.51.

4. Experimental investigation

In order to verify the calculation model presented in Section 3.3, an experimental investigation was carried out by Jansson [25]. In the experiments, the effect of using SFRC on the width and spacing of cracks formed in tie-rod elements subjected to monotonically increasing deformation was investigated. Additional data from results reported in the literature were also used to assess the applicability of the proposed model under restraint cracking. Furthermore, the material properties required to define the different parameters of the model were obtained from uniaxial tension tests and reinforcement pullout test performed by Jansson et al. [48]. In the following, a brief description of the different experimental tests considered is given including a summary of the main results.

4.1. Experiments by Jansson

In the study by Jansson, experiments were carried out using fibre reinforcement at various dosages, namely 0%, 0.25%, 0.5% and 1.0% by volume. A single type of steel fibre from Bekaert, Dramix® RC 65/35, was used in all the experiments. The fibres had hooked-ends and their length was 35 mm with a diameter of 0.55 mm. As for the concrete, a self-compacting concrete mix with a water cement ratio that ranged between 0.53 and 0.55 for the different mixes. The concrete mix composition for all mixes are presented in Table 1. The mean compressive strength was assessed from tests carried out on cylindrical specimens in accordance to the Swedish Standard SS-EN 12390-3:2009 and the results are presented in Table 2 for two different concrete ages, at 28 and 95 days.

Table 4.1. Concrete mix composition for all the mixes, in [kg/m^3]

Series	*0.0*	*0.25*	*0.5*	*1.0a*	*1.0b*
Cement CEM II/A-LL	359	361	362	368	357
Water	197	195	197	202	189
Sand 0 – 4 mm	679	748	808	693	661
Sand 0 – 8 mm	231	146	161	160	168
Gravel 5 – 8 mm	156	122	54	166	183
Gravel 8 – 16 mm	590	566	554	569	580
Filler (lime)	182	207	182	172	182
Super plasticizer	1.3	1.3	1.3	1.3	1.3
Fibres, Dramix® RC 65/35[a)]	0	14.1	34.5	77.5	65.5

[a)] Actual fibre content determined from washout controls, see [49].

Table 4.2. Mean concrete compressive strength, in [MPa]

	Series				
	0.0	*0.25*	*0.5*	*1.0a*	*1.0b*
$f_{cm,28d}$	59	59	58	59	50
$f_{cm,95d}$	65	64	63	65	55

- *Uniaxial tension tests*

Uniaxial tension tests were carried out at SP, the Technical Research Institute of Sweden, on cylindrical concrete specimens at the age of 165 days. The specimens used were cores extracted from larger specimens in order to eliminate the influence of the wall-effect on fibre orientation. Cracking was forced to occur at the centre of the specimens by sawing a 5 mm thick and 10 mm deep notch. Loading was introduced by gluing the top and bottom faces of the cylinders to the loading plates and the tests was carried out under displacement control at a constant rate of 0.005 mm/min. Crack widths were measured using three displacement transducers placed around the specimens separated by 120º. The geometry of the specimens and the setup of the tests is shown in Fig 4.1.

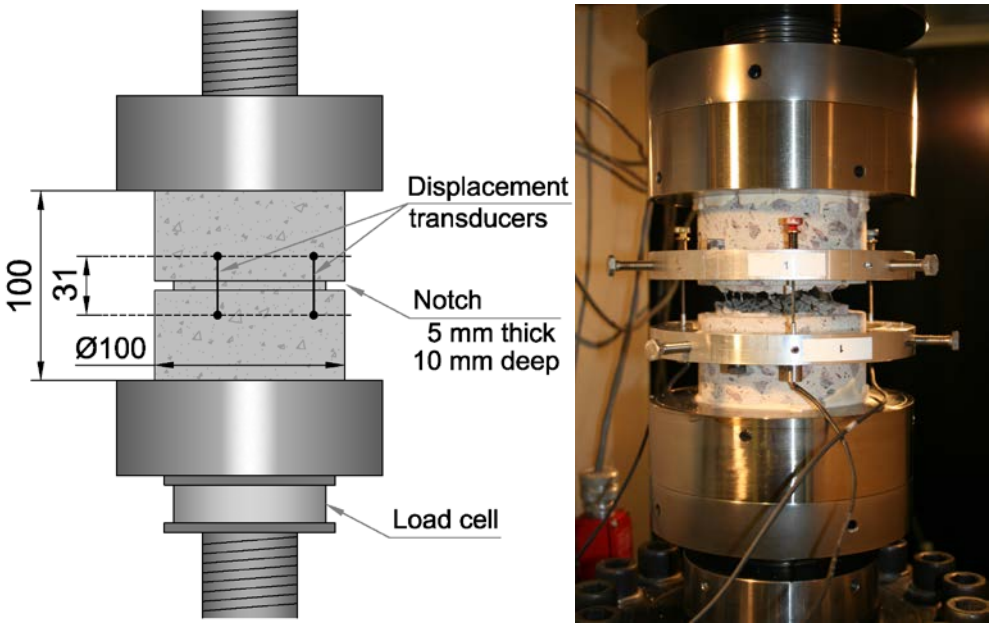

Figure 4.1 Specimen geometry and setup of the uniaxial tensile tests, from [25]*. All measurements are in mm.*

The results obtained from the uniaxial tension tests are curves expressing the relationship between the load applied to the specimen and the displacement measured over the notch. To obtain the stress-crack opening relationship, the stress was calculated as the ratio between the load and the effective concrete area at the notch. The crack opening was calculated, according to the RILEM recommendations [50], as the deformation that remains after deducing the deformation at the peak stress, where deformations are the average displacement from the three transducers. The obtained stress-crack opening curves are presented in Fig. 4.2(a) for all the mixes where each curve shows the average behaviour from five individual tests.

The initial region of the stress-crack opening curves, highlighted in Fig. 4.2(a), comprises the stress transferred through the crack for openings of up to one millimetre. This region, which is the most relevant part of the curve for crack control purposes since crack widths are always intended to remain well below that threshold, has been zoomed in Fig. 4.2(b). It is worth noting

that in this region, after an initial stress drop marked by the formation of a macro-crack, stresses rapidly reached an almost constant value.

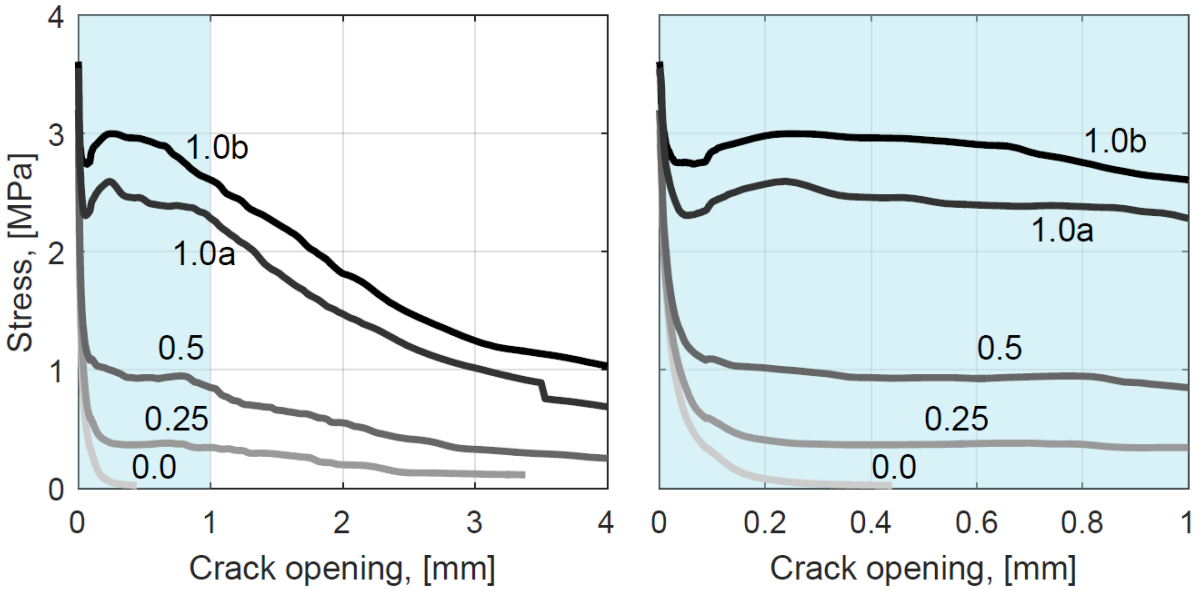

Figure 4.2 Average stress-crack opening curves from uniaxial tension tests. Each curve represents the mean value of five individual tests Labels are used to indicate the different series where the value corresponds to the fibre volume in the mix.

- *Pullout tests*

Pullout tests were carried out on cubic specimens reinforced with a single Ø16 mm bar in the centre of the cubes at the age of 95 days to determine the bond stress-slip relationship of the concrete-steel interface. The dimensions of the cubes were chosen taking into account considerations to ensure that the concrete cover was sufficiently small for surface strains to be measurable but large enough to avoid a premature splitting failure of the specimens without fibres. Thus, a cover of 48 mm was adopted. During the pullout tests, relative displacements were measured on both the active and passive ends of the bar. As for the uniaxial tension tests, the cubic specimens used for the pullout tests were sawn from larger concrete members to eliminate the preferential alignment of the fibres with the faces of the moulds. The geometry of the specimens and the setup of the tests is shown in Fig. 4.3.

In real structural members, bond stresses at the interface between steel reinforcement and concrete vary along the length of the bar. However, for short embedment lengths, i.e. when the bonded length is less than five times the bar diameter, the slip distribution along the bar can be considered as uniform and thus the bond stress adopts a nearly constant value along the bar. In such cases, the local bond stress, τ_b, may be calculated as an average bond stress, τ_{avg}, uniformly distributed on the embedded steel surface according to Eq. 4.1:

$$\tau_b \cong \tau_{avg} = \frac{P}{l_b \pi \emptyset} \tag{4.1}$$

where, P is the is the pulling force, l_b is the bonded length and $\pi\emptyset$ is the perimeter of the bar.

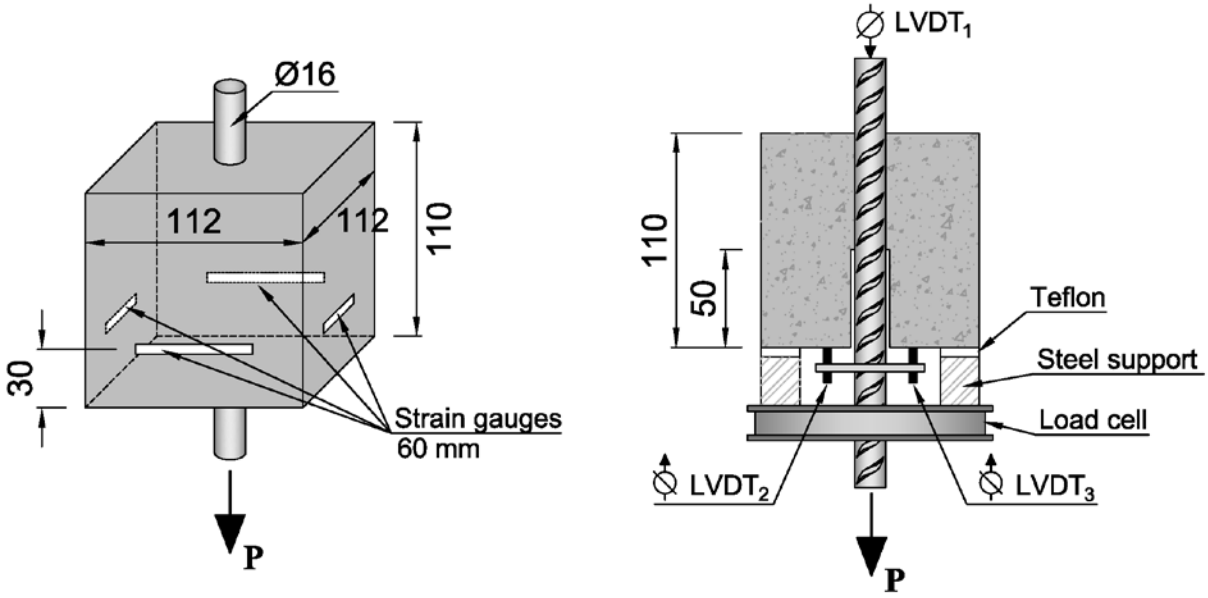

Figure 4.3 Specimen geometry and setup of the pullout test, from [48]*. All measurements are in mm.*

The main difference observed between the tested series was a progressive change in the failure mode from splitting in plain specimens (series 0.0) to pullout of the bar in specimens with increasing fibre content. A comparison of the average bond stress-slip curves before the peak stress obtained from the pullout tests is presented in Fig. 4.4(a). No significant difference was observed among the curves for the different series except for a slightly less stiff behaviour for the 1.0b series, which can be attributed to the comparatively lower strength of the concrete. The differences are eliminated when bond stresses are normalized to the compressive strength of the concrete, as shown in Fig. 4.4(b).

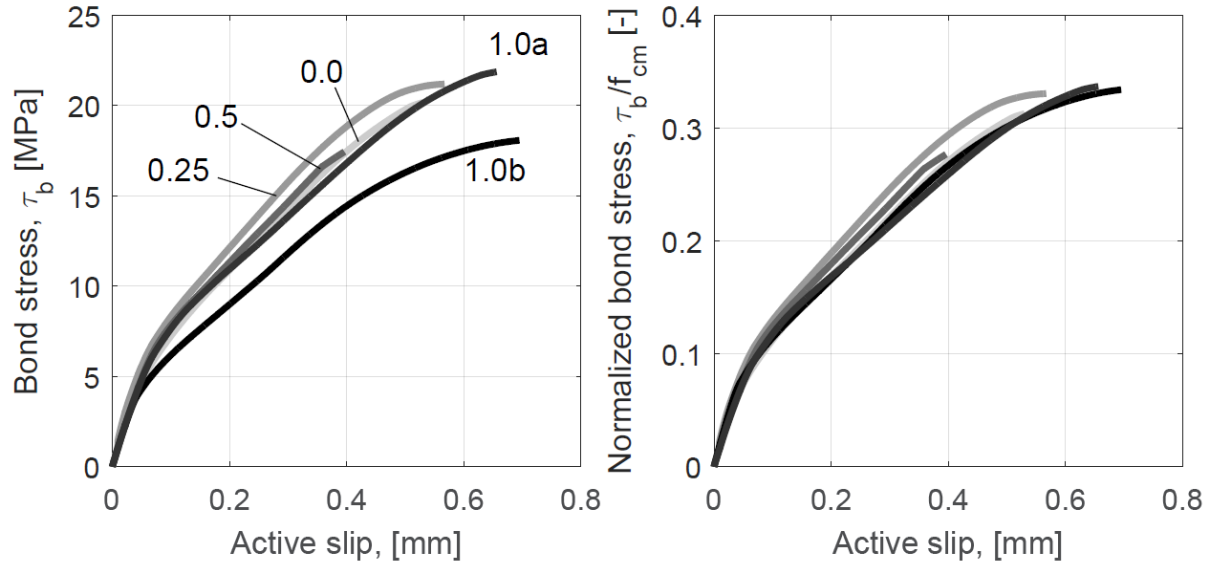

Figure 4.4 Average bond stress-slip curves for the ascending branch before the peak stress from the pullout tests (a) and the same results where the bond stress is normalized with respect to the mean compressive strength of each series (b). Each curve represents the mean value of five individual tests Labels are used to indicate the different series where the value corresponds to the fibre volume in the mix.

- *Tensile tests on tie-rod elements*

Jansson [25] performed tensile tests on tie-rod elements in order to study the formation of cracks under direct tension. The tie-rod specimens had an identical cross-section to that of the pullout specimens, i.e. a Ø16 mm centrically placed in a 112×112 mm square section resulting in a minimum cover of 48 mm, whereas in the longitudinal direction the tie-rod elements were 820 mm long. Similar to the previous specimens, the tie-rod elements were cut from larger slabs with dimensions 720×820×152 mm to eliminate the wall-effect on fibre orientation. The tests were carried out at a concrete age of between 28 and 37 days and they were performed under displacement control at a constant displacement rate of 0.007 mm/min up to yielding of the reinforcement. The elongation of the specimen was calculated as the difference between the displacement of the testing machine and the accumulated displacement measured by two groups of transducers placed between the machine and the specimens, on either end of the tie-rod elements. Furthermore, a full-field strain measurement was performed on all the tie elements using a non-contact optical deformation system based on Digital Image Correlation (DIC). This measurement system enabled tracking the formation and growth of tensile cracks during the tests. The geometry of the specimens and the setup of the test is shown in Fig. 4.5.

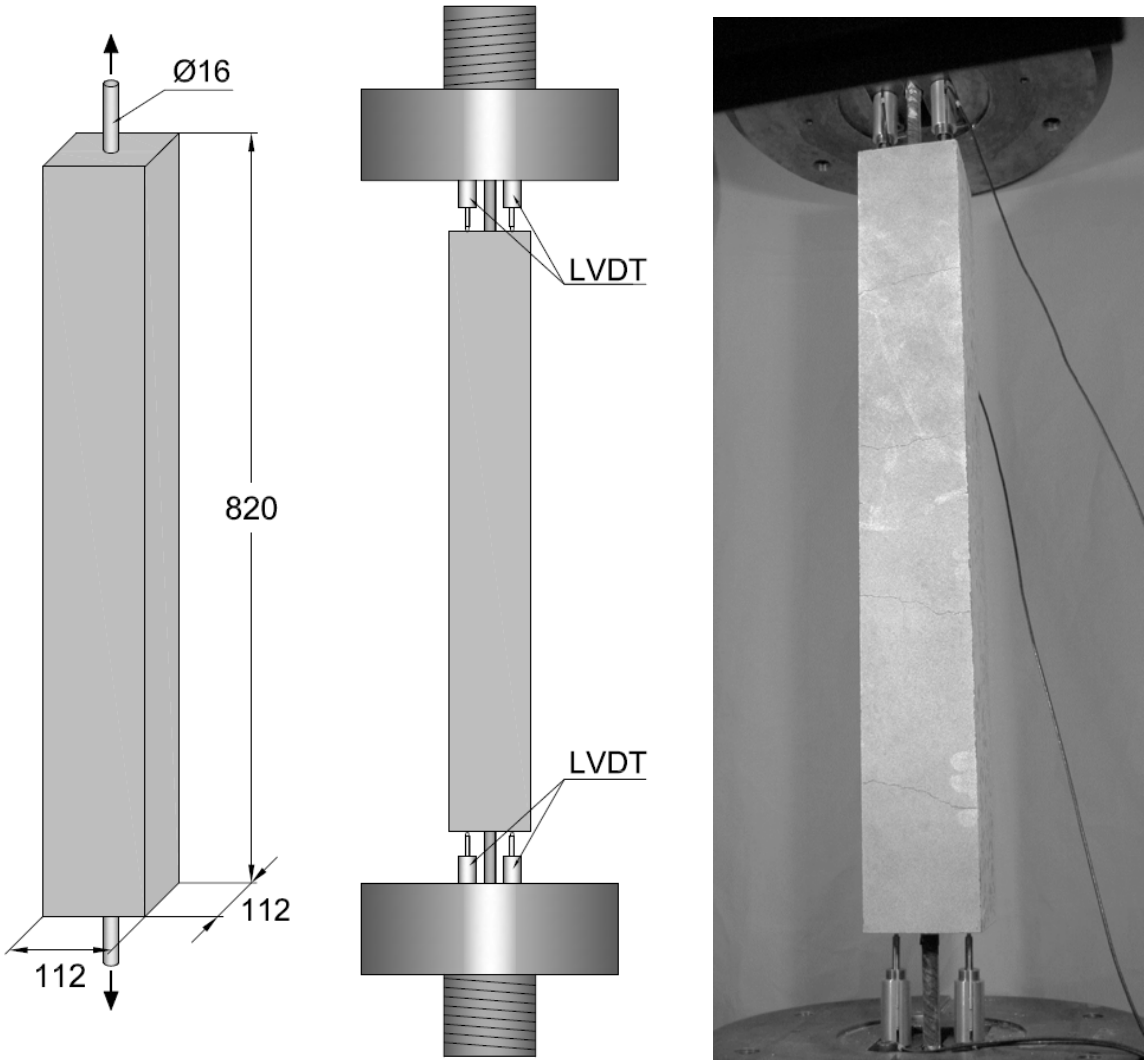

Figure 4.5 Specimen geometry and setup of the tensile tests on tie-rod element, from [25]. *All measurements are in mm.*

A comparison of overall behaviour of the different series is presented in Fig. 4.6 in the form of load-elongation curves. As observed, fibre reinforced specimens exhibited an increased tension-stiffening compared to plain concrete, particularly apparent in the series 1.0a and 1.0b, with the highest fibre content. Furthermore, the addition of fibres also resulted in an increase of the cracking load and a smoother response during the cracking stage with less sudden drops in the load, which can be attributed to the ability of fibres to transfer stresses through the cracks.

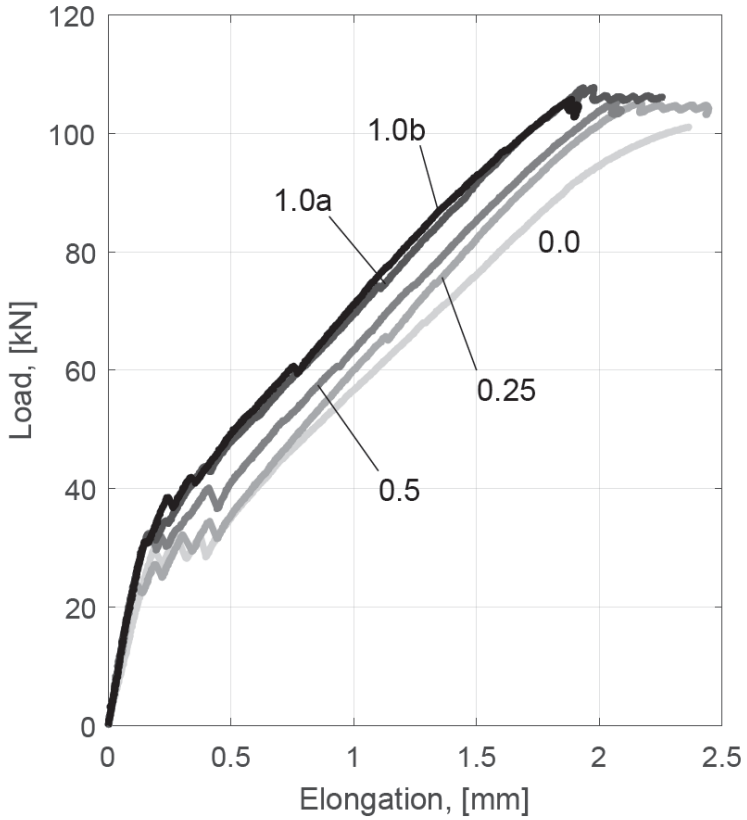

Figure 4.6 Example of the overall behaviour of the tie-rod elements for the different series.

Regarding transverse cracking, the final crack pattern achieved for each specimens at the end of the tests is presented in Fig. 4.7, where the side shown corresponds to the side used to monitor cracks with the DIC system. The average number of cracks and cracks spacing documented from the tests is presented in Table 4.3. As observed, fibres promoted an increase of the average number of cracks, which lead to a reduction of the average crack spacing. It should be noted that cracks in fibre reinforced specimens were also more irregular and, in many cases, transversal cracks did not fully propagate throughout the entire section.

Table 4.3 Average number of cracks and average cracks spacing determined from the observed crack patterns of the tie-rod elements at the end of the tensile tests.

Series	0.0	0.25	0.5	1.0a	1.0b
Avg. No. of cracks [a)]	4.4	5.2	5.4	5.6	5.6
Avg. Crack spacing	172	141	136	123	108

[a)] No. of cracks refers to the maximum number of cracks in any side of the specimen

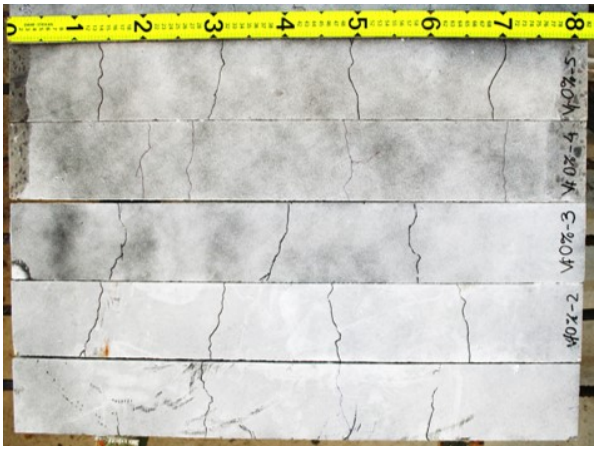

(a) Series 0.0

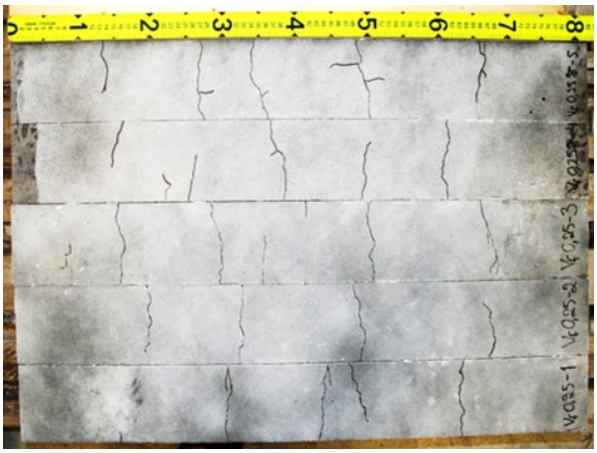

(b) Series 0.25

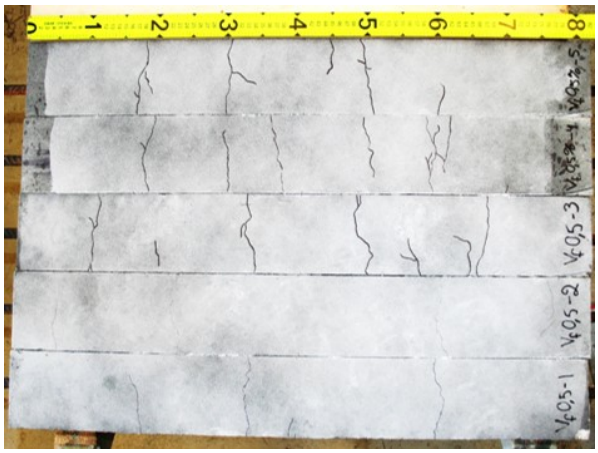

(c) Series 0.5

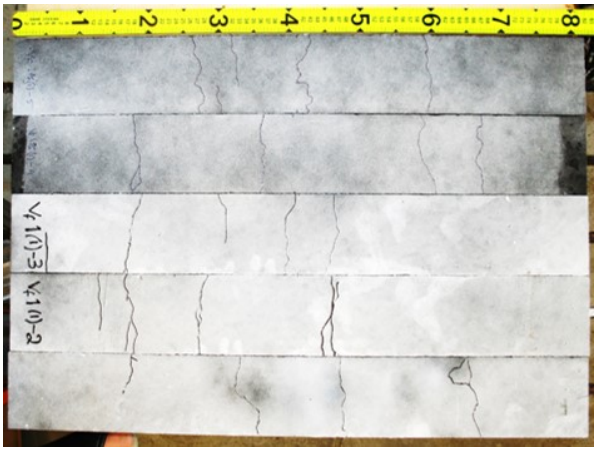

(d) Series 1.0a

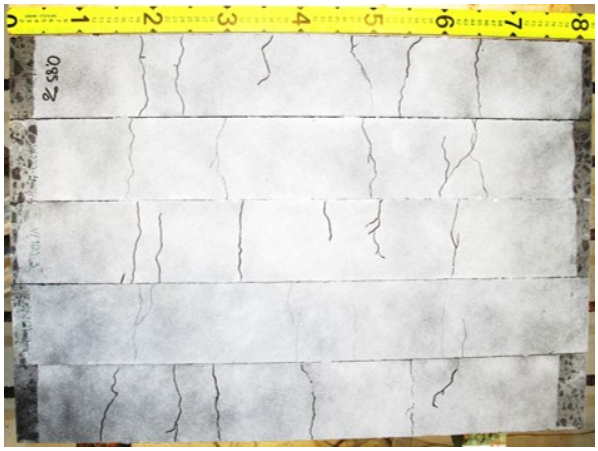

(e) Series 1.0b

Figure 4.7 Crack patterns for all the specimens tested showing the side that was monitored with the DIC system.

The determination of the crack width was performed based on the results obtained from the DIC measurements. However, the area covered by the DIC system included only the central 500 mm of the tie-rod elements. Thus, some cracks have not been considered for the determination of the average crack width.

Transverse cracks were measured creating a virtual gauge with the DIC system at the center of the crack on the surface of the measured side, as schematically shown in Fig. 4.8.

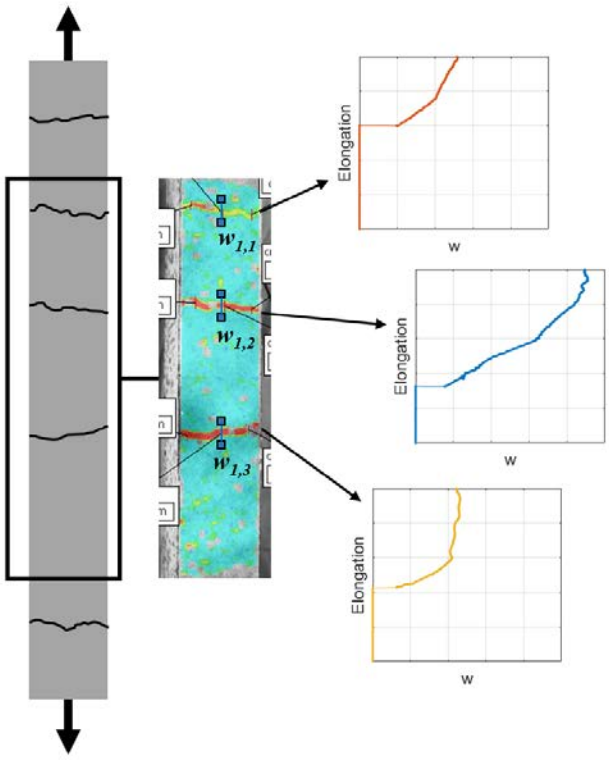

Figure 4.8 Determination of the crack width of individual transverse cracks in tie-rod elements for increasing specimen elongation from results obtain through the DIC system using virtual gauges.

The crack width of every crack captured by the DIC system was measured for increasing elongations up to the point where yielding of the rebar occurred. After removing data noise from the DIC measurements, the cracks were filtered using a moving average algorithm. The results are presented in Fig. 4.9 as a function of the applied tensile load for the five specimens in each series. Subsequently, an averaging process was carried out to determine the mean crack width, w_{mean}, of transverse cracks at different stress levels of the rebar. The averaging was performed over the number of measured cracks, n_{cr}, and over the number of specimens, n_s, according to Eq. 4.2:

$$w_{mean} = \frac{1}{n_s}\frac{1}{n_{cr}}\sum_{n_s}\sum_{n_{cr}} w_{i,j} \tag{4.2}$$

where $w_{i,j}$ is the i-th crack of the specimen j at a certain applied load. It should be noted that in the averaging process, the specimen number two of the 0.0 and 0.25 series was disregarded due to incomplete data, which could skew the results. Finally, the stress at the reinforcement was estimated, based on the applied load, P, and on the residual tensile strength, $f_{t,res}$, determined from the uniaxial tensile tests, according to Eq. 4.3:

$$\sigma_s = \frac{P - A_c \cdot f_{t,res}}{\frac{\pi \emptyset^2}{4}} \tag{4.3}$$

where σ_s is the stress of the reinforcement, $\emptyset$ is the bar diameter and A_c is the net concrete area of the tie-rod elements cross-section. The average crack width as a function of the tensile force and as a function of the stress level at the reinforcement is presented, for all series, in Fig. 4.10.

From Fig. 4.9, it can be seen that fibres had a clear impact on the total number of cracks formed. Whereas for plain concrete only between 2 and 3 were formed, for concrete elements with fibres generally 4 or more cracks appeared. The comparison of the maximum crack width between the series does not reveal large differences between the fibre reinforced mixes and their plain concrete counterpart, which can be most likely attributed to the formation of cracks in sections with locally decreased fibre contents. On the other hand, the average crack width, due to multiple cracking, is effectively reduced even for the lowest fibre content, as shown in Fig. 4.10(a). It should be noted that at an intermediate load of about 60 kN, the average crack width in hybrid reinforced elements is decreased from 0.4 mm to values between 0.26 and 0.18 mm, a reduction of 35% and 55%, respectively.

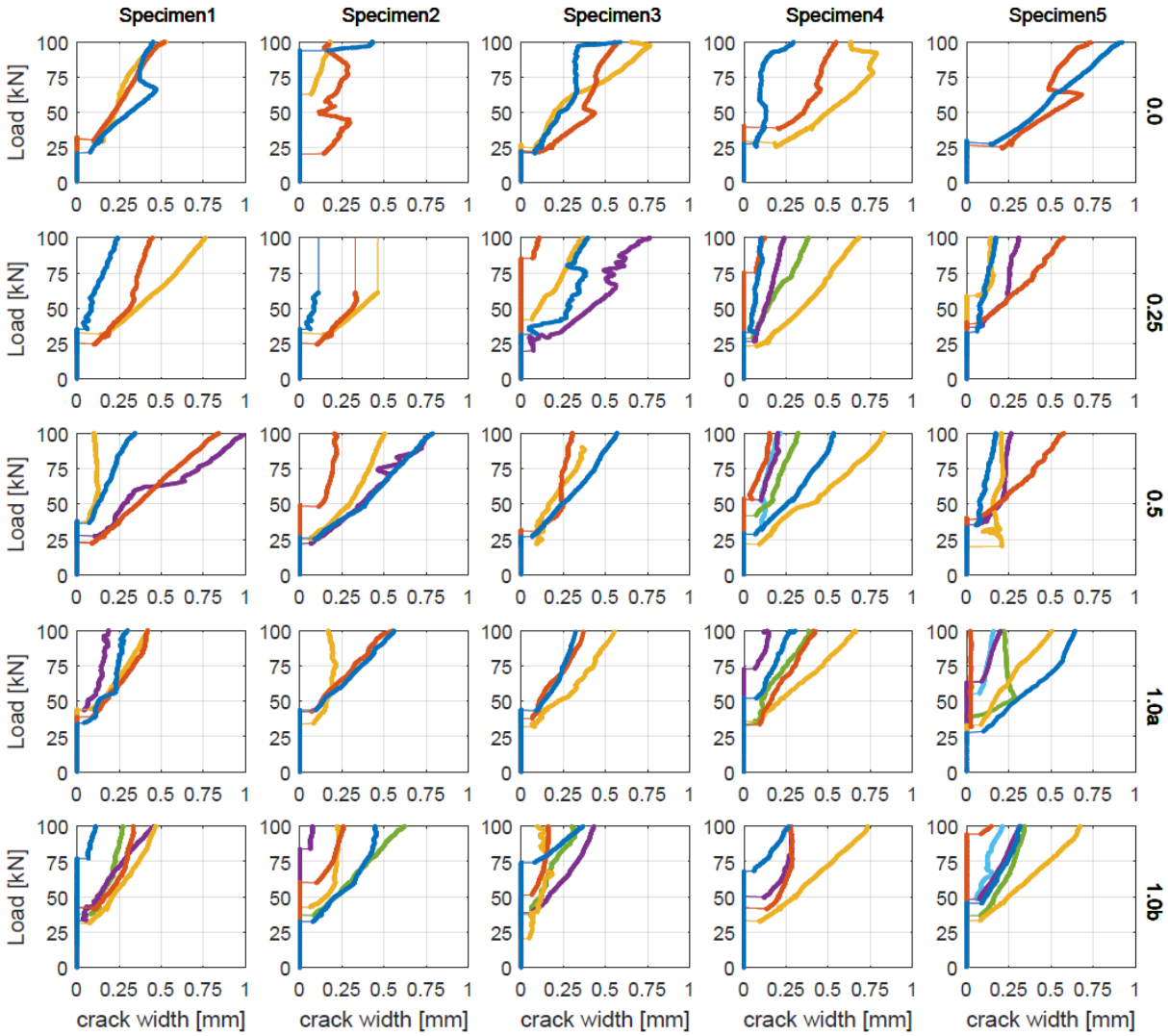

Figure 4.9 Crack width of individual transverse cracks as a function of applied tensile load obtained from measurements performed with the DIC system for all the specimens in each series (after filtering).

Conversely, when compared to the calculated reinforcement stress, the crack width in elements with fibre reinforcement does not differ from that of plain concrete elements. This observation suggests that the beneficial effect of fibres on the reduction of crack width, in FRC exhibiting post-crack tensile-softening behaviour, can be evaluated in terms of their ability to reduce the stress in the conventional reinforcement.

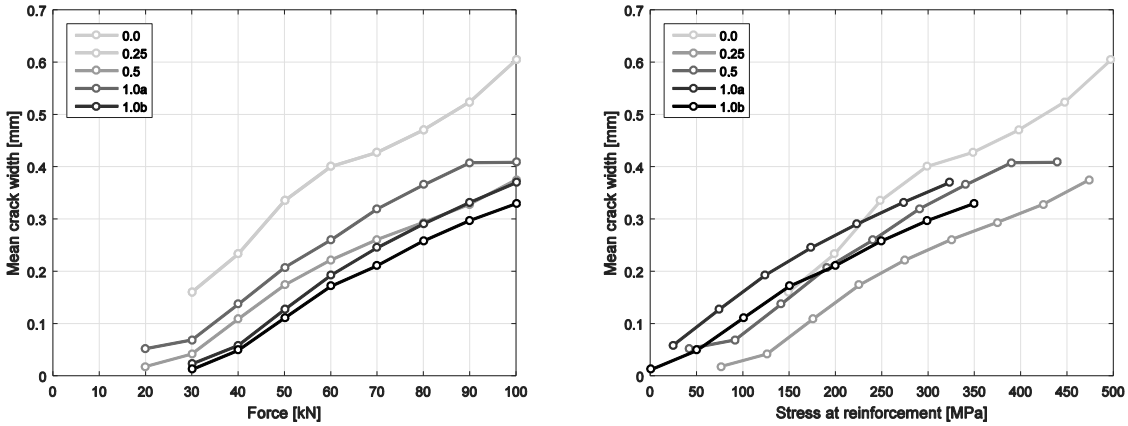

Figure 4.10 Average crack width as a function of the stress at the reinforcement.

4.2. Experiments by Nejadi and Gilbert

The experiments by Nejadi and Gilbert [42] are presented in this section in order to assess the validity of the restraint cracking model presented in Section 3.3. Nejadi and Gilbert tested a set of eight fully restraint slabs with four different reinforcement layouts to measure the effect of drying shrinkage on restraint cracking. The specimens were 2000 mm long by 600 mm wide prismatic slabs with a nominal thickness of 100 mm. The slabs were monolithically connected via 330 mm long splayed sections to two end concrete blocks, which were firmly anchored to a strong floor to provide effective restraint to the shrinkage strain of the prismatic portion. Moreover, two 75 mm wide notches were formed at the centre of the prismatic region to enforce the first crack to occur at the position. The geometry and dimensions of the slabs are illustrated in Fig. 3.11 together with a general view of the slabs during the tests.

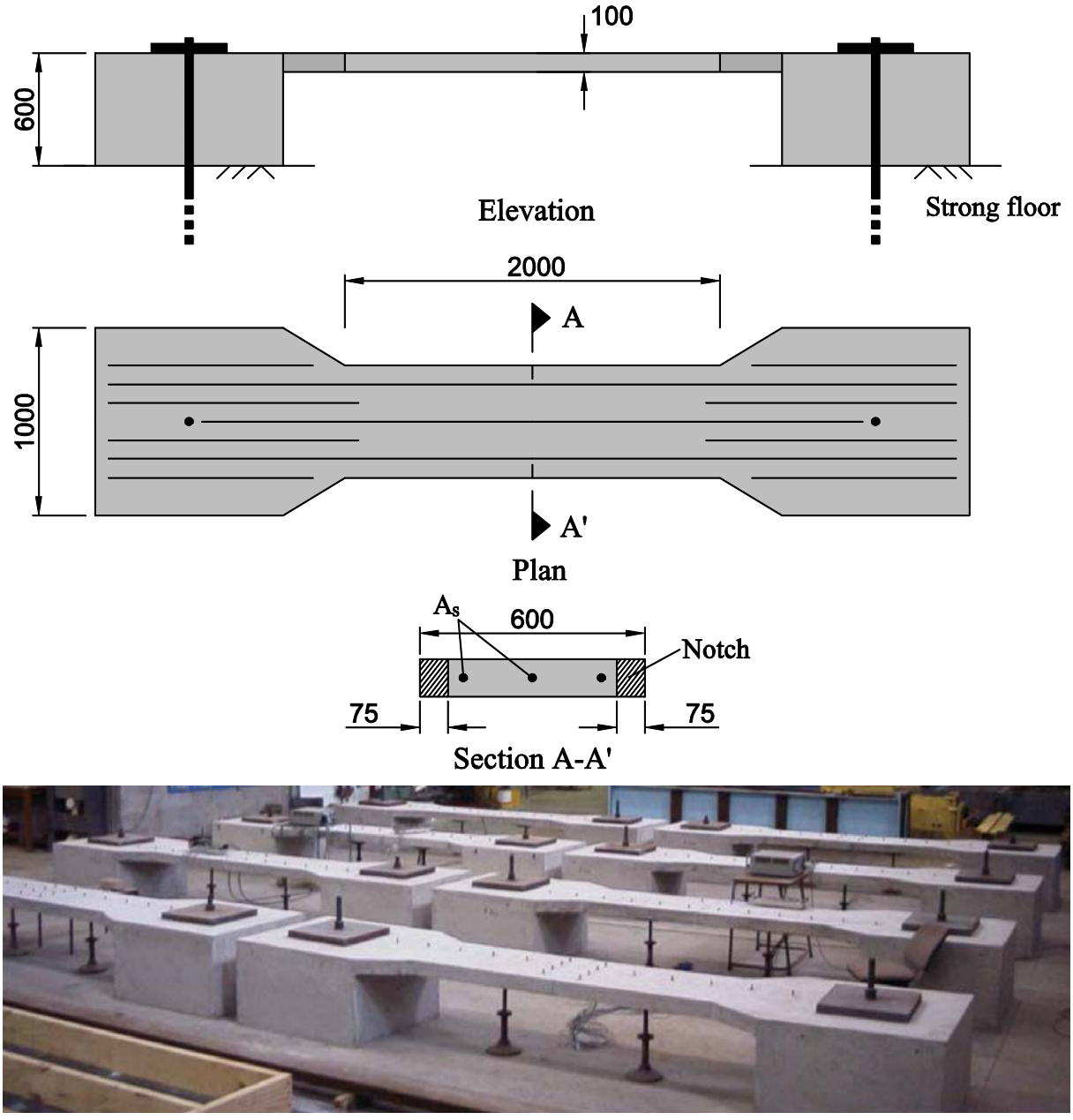

Figure 4.11 Geometry and dimensions of the restrained slab specimens and general view of the slabs in during the testing period, from Nejadi and Gilbert [42].

The parameters investigated through the variation of the reinforcement layout were the number of bars, from 2 to 4, the bar diameter, either 10 or 12 and the reinforcement area. The nomenclature and details of the reinforcement and cross-section of each slab are included in Table 4.4.

Table 4.4 Details of slab specimens

Specimen	Number of bars, n [-]	Bar diameter, Ø [mm]	Reinforcement Area, A_s [mm^2]	Actual thickness [mm]
S1a	3	12	339	102.2
S1b	3	12	339	99.8
S2a	3	10	236	101.6
S2b(#)	3	10	236	98.3
S3a	2	10	157	99.2
S3b	2	10	157	99.3
S4a	4	10	314	100.5
S4b	4	10	314	101.1

(#) The slab Sb2 was cast from a different concrete batch (Batch II).

Two different concrete batches were used to cast the slabs (see Table 4.4). Companion specimens were cast simultaneously with the slabs to determine the material properties throughout the period of the testing. The measured properties included compressive strength, elastic modulus, direct tensile strength and creep coefficient. The evolution of the drying shrinkage strain was also measured using unrestrained specimens of similar dimensions to the restrained slabs. The results of these tests as reported in [42] are presented in Table 4.5.

Table 4.5 Material properties for the concrete Batches I and II, from Nejadi and Gilbert [42].

Material properties	Batch I	Batch II
Compressive strength at (7) and 28 days [MPa]	(13.7) 24.3	(17.4) 28.4
Splitting tensile strength at (7) and 28 days [MPa]	(1.55) 1.97	(1.60) 2.10
Elastic modulus at (7) and 28 days [MPa]	(17130) 22810	(18940) 23210
Shrinkage strain at 122 days [με]	457	495*
Creep coefficient at 122 days [-]	0.98	1.16*

*The shrinkage strain and creep coefficient of Batch II corresponds to 150 days

The restraint cracking tests were carried out for a total period of 150 days under which the specimens were kept undisturbed while the number of cracks, the crack spacing, crack width and steel and concrete strains were monitored. Furthermore, due to drying shrinkage in the end blocks, the prismatic part of the slabs suffered a longitudinal elongation, Δu. The total specimen elongation, observed number of cracks, mean crack spacing and crack width, and the maximum steel stress at the first crack and concrete stresses in uncracked regions (derived from steel strains) are presented in Table 4.6 as reported by Nejadi and Gilbert.

Table 4.6. Experimental results of the restraint shrinkage tests, from Nejadi and Gilbert [42].

Specimen	Elongation, Δu [mm]	Number of cracks, n_{cr}	Mean crack spacing, s_{rm} [mm]	Mean crack width, w_m [mm]	Max steel stress, σ_s [MPa]	Max concrete stress, σ_c [MPa]
S1a	0.305	4	670	0.21	273	1.77
S1b	0.383	4	403	0.18	190	1.41
S2a	0.309	3	674	0.30	250	1.13
S2b(#)	0.315	3	700	0.31	290	1.46
S3a	0.402	1	-	0.84	532	1.45
S3b	0.419	2	997	0.50	467	1.31
S4a	0.245	3	783	0.23	270	1.64
S4b	0.162	3	995	0.25	276	1.71

(#) The slab Sb2 was cast from a different concrete batch (Batch II).

5. Analytical study of test specimens

In this chapter, the analytical model described in Section 2.5 is compared to the experimental results presented in Chapter 3 and other analytical formulations. First, the experiments by Jansson et al. [48] are used to assess the accuracy of the proposed expression for the relationship between steel stress and crack width This expression is also compared to the combinations of maximum steel stress and bar diameter for minimum reinforcement requirements in elements subjected to restraint cracking as recommended in the Eurocode 2 [34] as well as the results from another existing analytical model for hybrid reinforcement by Niemann [51]. Subsequently, the slabs subjected to restrained shrinkage tested by Nejadi and Gilbert [42] are also utilized to validate the restraint cracking model.

5.1. Steel stress – crack width relationship

As previously shown in Section 3.3, the proposed restraint cracking model is based on a relationship between stress at the reinforcement and crack width, which in turn is derived from the bond stress-slip relationship assumed between steel and concrete. In this case, the assumed bond-slip relationship is taken according to the expression given in the current Model Code 2010 [35], which is compared in Fig. 5.1 to the experimental results from the pull-out tests by Jansson et al. [48], taking an average concrete strength at 95 days of 64 MPa. As observed, the initial part of the bond-slip relationship yields a satisfactory agreement with the experimental results up to a slip of about 0.2 mm, which was found to be the most relevant part of the bond-slip relationship for crack width calculations. Thereafter, the suggested relationship underestimates the experimental results. The higher stiffness observed in the experiments could be attributed to the use of self-compacting concrete, whereas the analytical expression is derived for normal concrete.

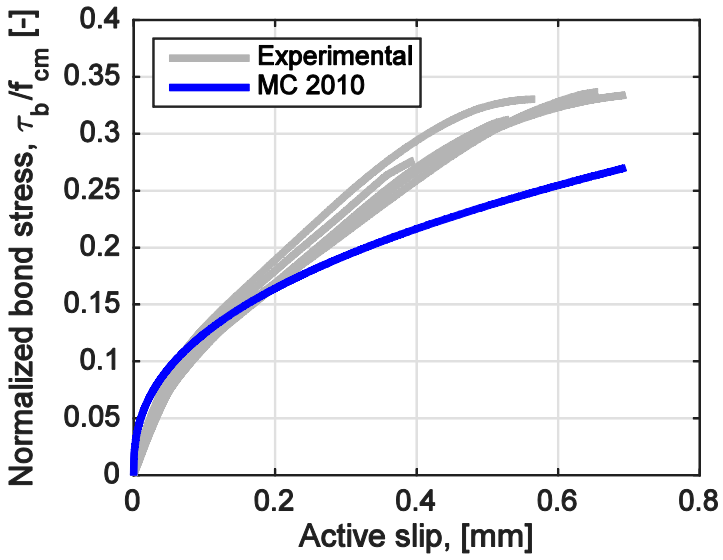

Figure 5.1. Normalized bond stress-slip relationships from pull-out experiments by Jansson et al. [48] *and from analytical expression given in Model Code 2010* [35] *for f_{cm} = 64 MPa.*

Using Eq. 3.53, the mean crack width has been calculated for a steel stress ranging from 0 to 500 MPa. The results are depicted in Fig. 5.2 together with the mean crack width results from

the tensile tests on tie-rod elements presented in Section 4.1, as a function of the steel stress, for both plain concrete and fibre reinforced concrete. Overall, a good agreement is observed for both cases, indicating Eq. 3.53 can be used to predict the mean crack width from reinforcement stress. For plain concrete, even though the experimental and analytical results do not fully agree, the ascending trend suggested by the model is also exhibited by the experimental mean crack width. On the other hand, for fibre reinforced mixes, the experimental results indicate that, contrary to what the model predicts, the increase of crack widths tended to stabilise with increasing steel stress. This effect could be attributed to the fact that several cracks initiating at different load levels are considered for the calculation of the mean crack width, some of which actually stop opening or even slightly reclose upon the appearance of new cracks. Moreover, it can be also seen that, for relatively low steel stresses, the analytical model tends to underestimate slightly the crack width.

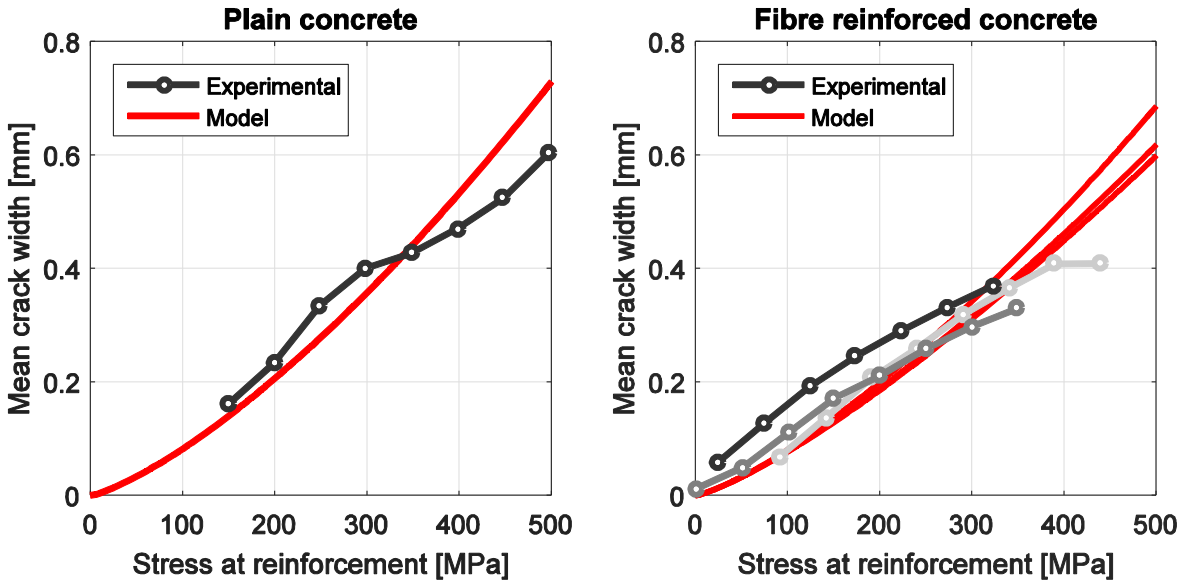

Figure 5.2. Comparison of experimental results and analytical expression for the steel stress- mean crack width relationships for plain concrete (left) and fibre reinforced concrete (right).

To neglect the effect of cracks that re-close when new cracks form, the most active crack in the RC tie elements, i.e. the crack exhibiting the largest crack width and monotonic opening during the loading procedure, has also been compared to the analytical expression of the crack width as a function of the steel stress for plain concrete (see Fig. 5.3) and for the different fibre reinforced concrete mixes (see left plot in Fig. 5.4 to Fig. 5.7). As observed, for plain concrete, the general trend is very well captured by the analytical expression although a significant scatter is clear in the experimental curves, which increases with increasing steel stress. For fibre reinforced concrete mixes, however, an underestimation of the crack width can be observed, which becomes more apparent for higher residual tensile strengths, $f_{t,res}$. This behaviour is most likely due to the fact that the widest cracks occurred in sections of the RC tie elements where the fibre density was locally decreased compared to that of the uniaxial tensile test, hence a lower actual residual strength might have been more suitable to analyse those sections.

The right plot in Fig. 5.4 to Fig. 5.7, shows the same type of results but for a less active crack, i.e. individual cracks that showed monotonic opening but with a near average crack width. As observed, the behaviour of the fibre reinforced concrete mixes is much closer to that predicted

by the analytical model when a less active crack is used for the comparison, except for the series with 0.25% vol. fibre dosage, in which the most active crack yielded a better agreement.

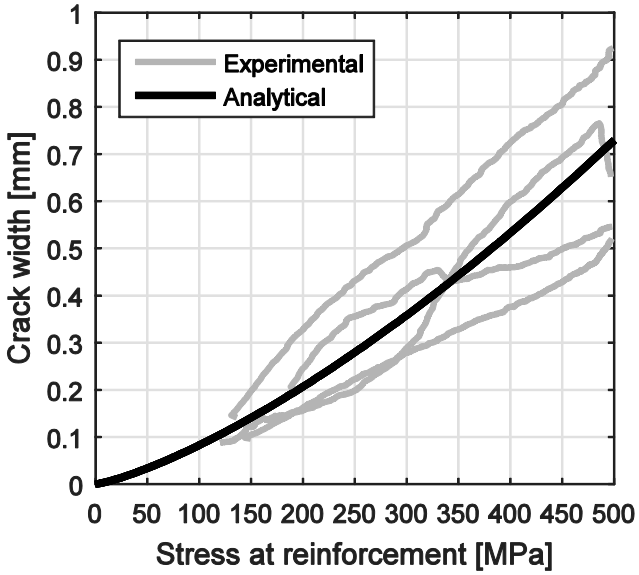

Figure 5.3. Comparison of experimental results and analytical expression for the steel stress - max crack width relationships for plain concrete.

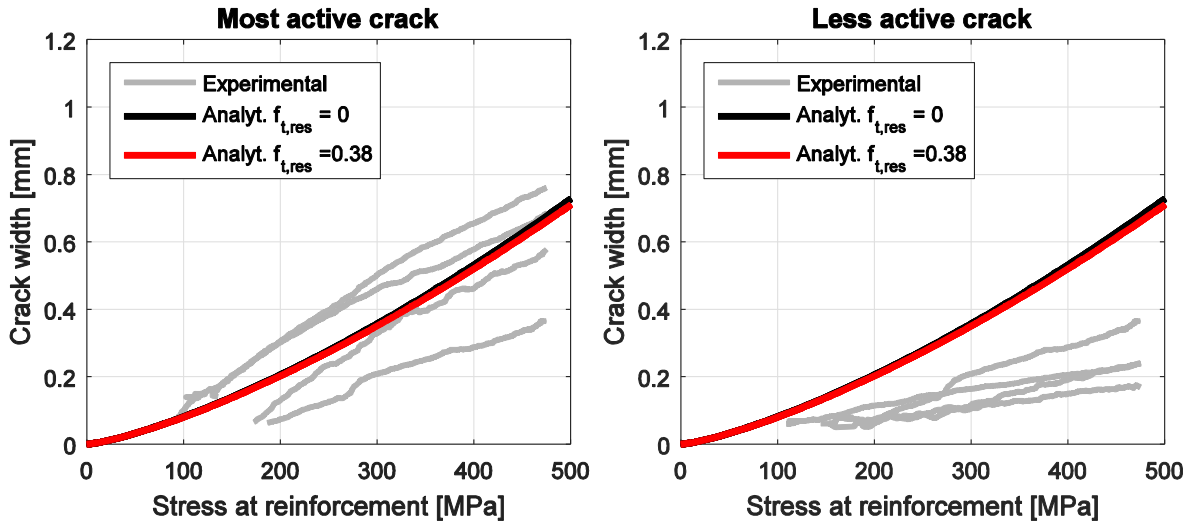

Figure 5.4. Comparison of experimental results and analytical expression for the steel stress-crack width relationships for the 0.25% fibre reinforced concrete series. Most active crack (left) and a less active crack (right).

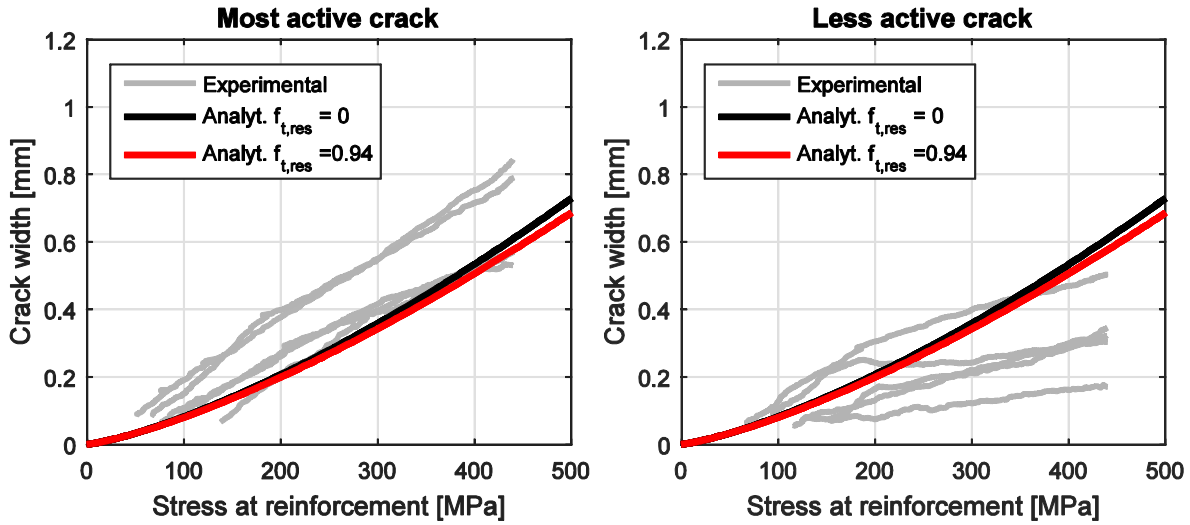

Figure 5.5. Comparison of experimental results and analytical expression for the steel stress-crack width relationships for the 0.5% fibre reinforced concrete series. Most active crack (left) and a less active crack (right).

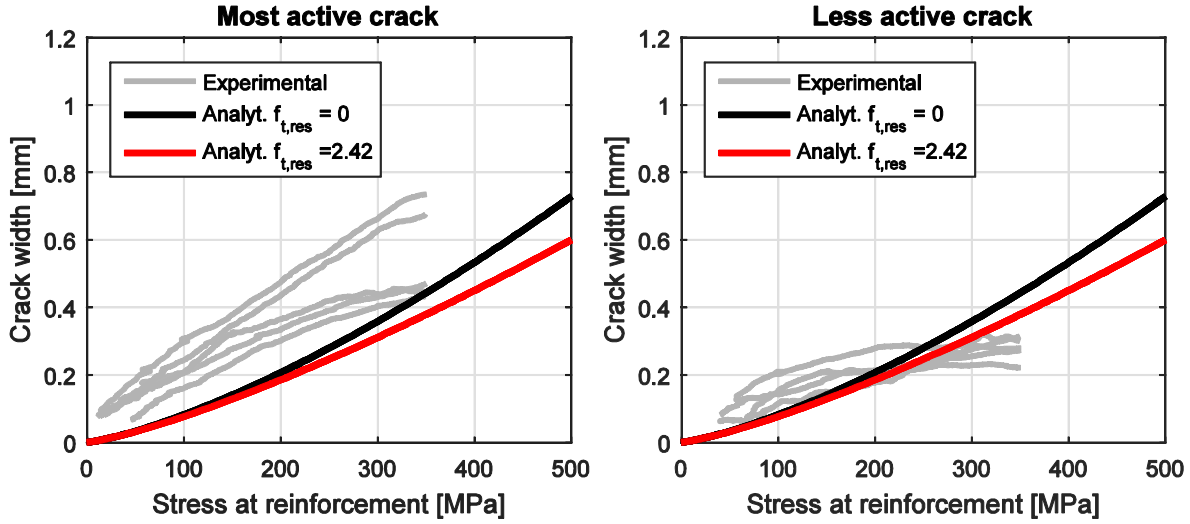

Figure 5.6. Comparison of experimental results and analytical expression for the steel stress-crack width relationships for the 1.0% (a) fibre reinforced concrete series. Most active crack (left) and a less active crack (right).

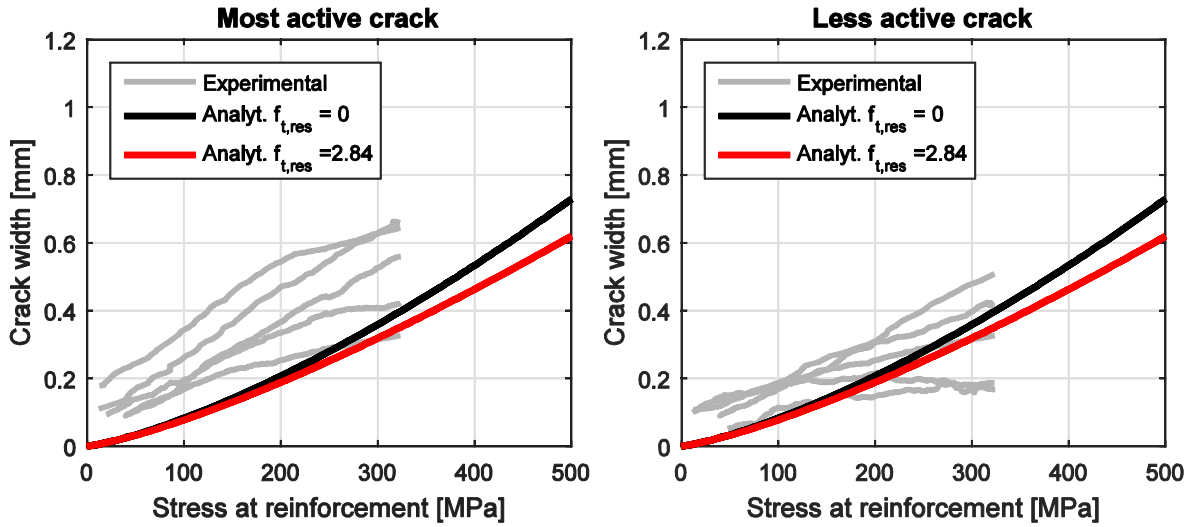

Figure 5.7. Comparison of experimental results and analytical expression for the steel stress-crack width relationships for the 1.0% (b) fibre reinforced concrete series. Most active crack (left) and a less active crack (right).

The analytical relationship between stress at the reinforcement and crack width provided by Eq. 3.53 has been also compared in Fig. 5.8 to the combinations of maximum steel stress and bar diameter for minimum reinforcement requirements in elements subjected to restraint cracking prescribed by the Eurocode 2 [34] to limit the characteristic crack width. As observed, the results of the analytical model are in agreement with the recommendations of the Eurocode 2, although for a given aimed crack width, the Eurocode 2 prescribes a slight lower tensile stress at the reinforcement. Due to the lack of specific calculations, it should be expected that the approach adopted by the Eurocode 2 to be conservative, hence a more restrictive limitation of the steel stress.

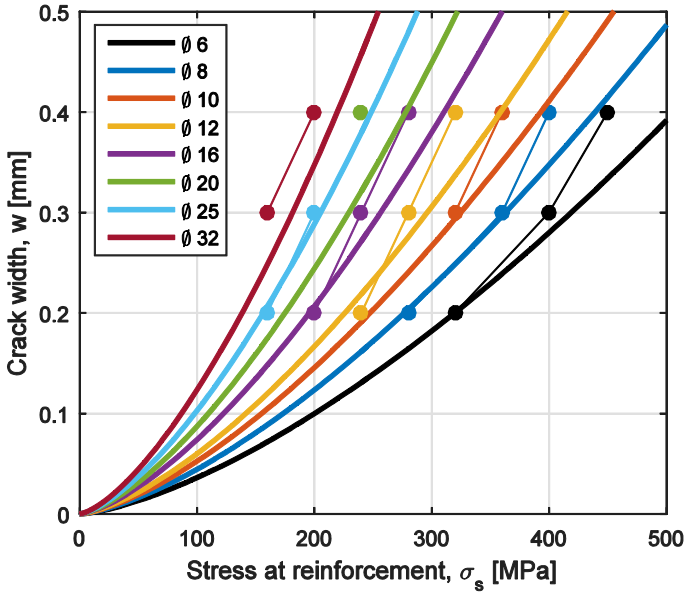

Figure 5.8. Relationship between steel stress at the reinforcement and mean crack width as a function of the bar diameter calculated from the analytical model (lines), compared to the maximum bar diameter prescribed by the Eurocode 2 to achieve characteristic crack widths of 0.2, 0.3 and 0.4 mm as a function of the steel stress (markers). Input values for the concrete are f_{cm} = 38 MPa and f_{ctm} = 2.9 MPa.

Finally, the expression of the relation between crack width and steel stress has been compared in Fig. 5.9 to the analytical predictions of a model for hybrid reinforced concrete included in a report by Niemann [51]. In this case, the predicted mean crack width is plotted as a function of the reinforcement ratio for different theoretical fibre dosages. The variation of the fibre dosage is introduced in the model through a parameter α_f that represents the ratio between the residual tensile strength of the concrete, $f_{t,res}$, and its tensile strength f_{ct}. Thus, plain concrete has a value of $\alpha_f = 0$, which increases with increasing fibre dosage. In Fig. 5.9, the relationship between reinforcement ratio and mean crack width is shown for an 8 mm bar diameter. As observed, the two models show an excellent agreement, which further supports the applicability of the expression given by Eq. 3.53 to predict the crack width in elements with hybrid reinforcement. On the other hand, the results in Fig. 5.9 clearly show the beneficial effect of fibres, which could be used to achieve the same crack width with half the amount of conventional reinforcement, an effect that could potentially be even greater for larger reinforcement bar diameters.

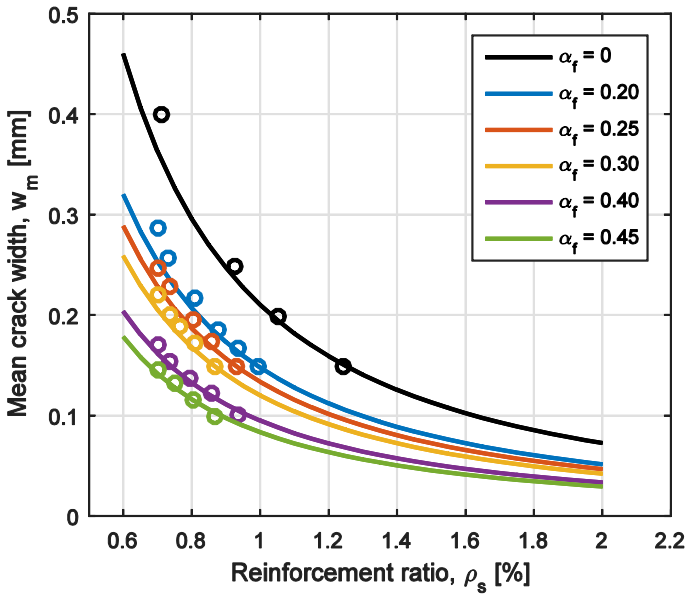

Figure 4.9. Relationship between reinforcement ratio and mean crack width at the cracking load as a function of the residual tensile strength expressed as the ratio of tensile strength, calculated by the proposed analytical model (lines) and a model by Niemann [51] *(markers). Input values for the concrete are f_{cm} = 38 MPa and f_{ctm} = 2.9 MPa and bar diameter Ø = 8 mm.*

5.2. Analysis of restraint cracking

In this section, the restraint cracking model is validated with the experimental results from Nejadi and Gilbert [42]. Unfortunately, to the author's knowledge, no experimental results are available regarding restraint cracking in elements with hybrid reinforcement. Therefore, the restraint cracking model is validated only for plain concrete.

By using the analytical model mathematically described by Eq. 3.47, Eq. 3.52 and Eq. 3.53, presented in Section 3.3, the total number of cracks (n_{cr}), the final average crack width (w), and the final maximum stress at the reinforcement (σ_s) have been calculated for each of the slab specimens tested by Nejadi and Gilbert. These quantities are compared to the experimental results reported in Table 4.6 and the comparison is presented in Fig. 5.10 – Fig. 5.12 as well as in Table 5.3 where the relative error of the model is also included.

The input parameters for the model common to all the slabs are included in Table 5.1 and Table 5.2. The remaining parameters used in the model, namely the slab height and the corresponding reinforcement layout, i.e. number and size of reinforcement bars, were taken according to the reported values as presented in Table 4.4. The shrinkage strain used as an input was modified to include the elongation of the slab elements due to the displacement of the restraining supports. Moreover, it should be noted that the values for the material properties of the concrete are taken according to the experimentally determined values at a concrete age of 28 days, except for the tensile strength for which the value at 7 days was taken instead. This choice is made based on the results by Nejadi and Gilbert, who reported that the first crack occurred earlier than 7 days after the initiation of the experiments. Furthermore, the width of the slab for the slabs Sa3 and Sb3, both of which featured a reinforcement layout consisting on only 2Ø10 spaced at 300 mm, was reduced to an effective width, b_{ef}, according to the following expression:

$$b_{ef} = \min\left\{n_{bars} \cdot 5\left(c + \frac{\emptyset}{2}\right), b_{tot}\right\} \tag{5.1}$$

where c is the concrete cover. This expression is based on the distance used in the Eurocode 2 [34] to describe the variation of the crack width at the concrete surface relative to the distance from the rebar and the reduction of the width is motivated by the fact that with a very large rebar spacing, the distribution of stresses in the concrete can no longer be assumed uniform and, therefore, the concrete section might partially crack near the rebar location for a total axial force lower than the calculated cracking load taking into the full section.

Table 5.1. Geometrical parameters used as input for the analytical restraint cracking model.

Geometrical parameters	
Width, b_c [mm]	600
Length, L_c [mm]	2000
Degree of restraint, R [-]	1

Table 5.2. Material properties used as input for the analytical restraint cracking model.

Material properties	
Concrete	Batch I / Batch II
Mean compressive strength, f_{cm} [MPa]	24.3 / 28.4
Mean tensile strength, f_{ctm} [MPa]	1.55 / 1.60
Elastic Modulus, E_c [MPa]	22810 / 23210
Creep coefficient., φ_c [-]	0.98 / 1.16
Shrinkage strain, ε_{cs} [με]	457 / 495
Steel reinforcement	
Yield stress, f_y [MPa]	550
Elastic Modulus, E_s [MPa]	200 000

In Fig. 5.10, the total number of cracks formed in the slabs investigated are compared to the total number of cracks predicted by the model. As observed, the model predicted the exact number of cracks in 6 out the 8 cases, being the error in the remaining two cases an overestimation of just one crack more than the actual total number of cracks.

In Fig. 5.11 and Fig. 5.12 a comparison of the mean crack width at the end of the experiments and maximum steel stress are presented for the experimentally measured and analytically predicted values, respectively. The degree of agreement between experimental and analytical results in Fig. 5.11 and Fig. 5.12 decreases with increasing distance to the diagonal, points located above and under the diagonal indicating an overestimation and underestimation of the model, respectively. As observed, the model successfully reproduces the general trend of the experimental results, although it consistently overestimates the experimental results of both crack width and steel stress, which is on the safe side.

As shown in Table 5.3, the average error made by the model is 34% for the mean crack width and 20% for the steel stress, values that are in the same range of the error made by other similar models. However, further experiments are required to assess the accuracy and reliability of the proposed model to predict the crack width and steel stress due to restraint cracking in concrete elements with hybrid reinforcement.

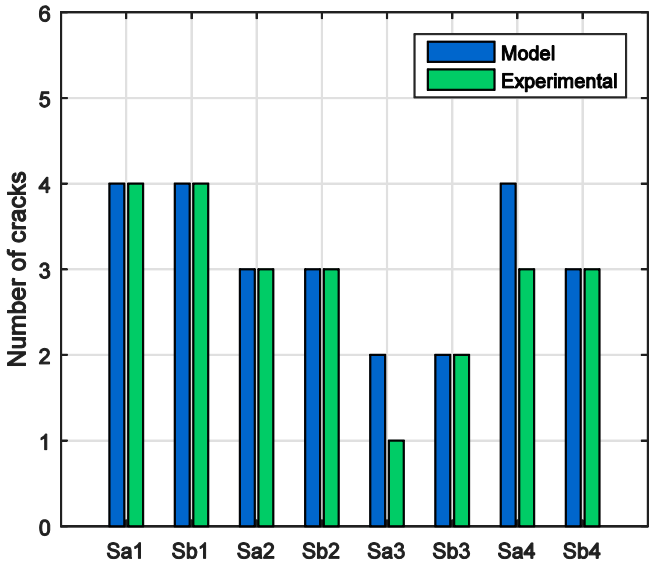

Figure 5.10. Total number of cracks developed in the restrained slabs investigated by Nejadi and Gilbert [42]. *Comparison of experimental and analytical results.*

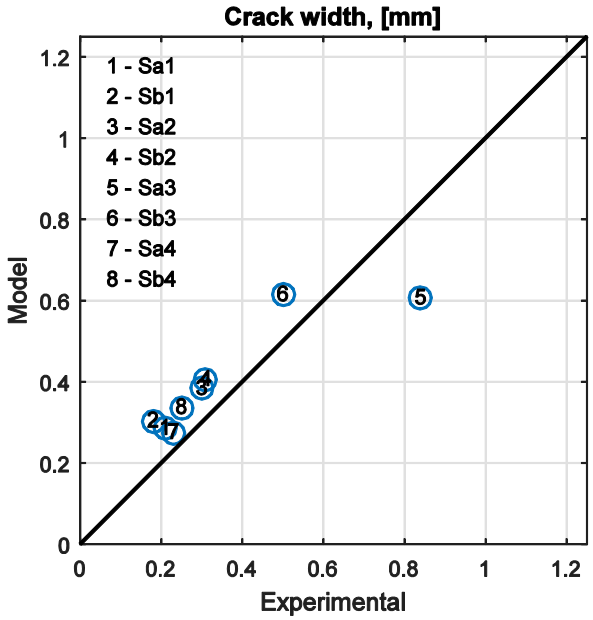

Figure 5.11. Final mean crack width in the restrained slabs investigated by Nejadi and Gilbert [42]. *Comparison of experimental and analytical results.*

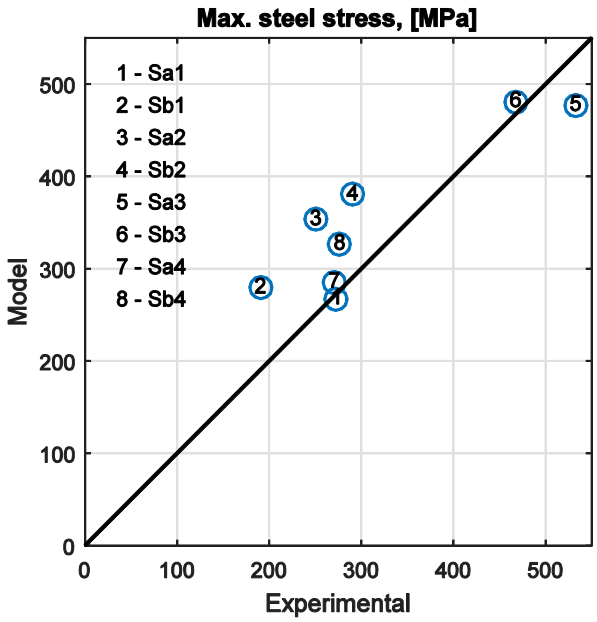

Figure 5.12. Final maximum stress in the reinforcement in the restrained slabs investigated by Nejadi and Gilbert [42]*. Comparison of experimental and analytical results.*

Table 5.3. Experimental and analytical values of the different compared parameters for the 8 slab specimens investigated by Nejadi and Gilbert [42]*, including the average error of the model.*

	Number of Cracks			Mean crack width [mm]			Max. Steel stress [MPa]		
	Exp.	Model	Error(%)	Exp.	Model	Error(%)	Exp.	Model	Error(%)
Sa1	4	4	0	0.21	0.29	36	273	267	-2
Sb1	4	4	0	0.18	0.30	69	190	279	47
Sa2	3	3	0	0.30	0.38	28	250	353	41
Sb2	3	3	0	0.31	0.41	31	290	380	31
Sa3	1	2	100	0.84	0.61	-28	532	477	-10
Sb3	2	2	0	0.50	0.61	23	467	481	3
Sa4	3	4	33	0.23	0.27	20	270	285	6
Sb4	3	3	0	0.25	0.34	34	276	326	18
		Average=	17		Average=	34		Average=	20

6. Conclusions and need for further research

6.1. Concluding remarks

In the present work, the cracking behaviour of hybrid reinforced concrete elements has been investigated, both experimentally and through a literature review, to provide a basis for design and execution recommendations as well as to determine the effectiveness of hybrid reinforcement for crack control in concrete structures. The following conclusions can be drawn:

- The calculation of crack width in current design codes and recommendations is limited to load-induced cracks, whereas a simplified approach, consisting in providing minimum reinforcement amounts and limiting the maximum bar diameter, is commonly adopted for crack control in reinforced concrete elements due to restraint forces.

- Different models for the calculation of crack width due to restraint forces in reinforced concrete members have been proposed by some authors. However, the proposed models introduce some simplifications regarding some crucial parameters, such as the bond-slip relationship between steel and concrete, which might limit the applicability of these models to predict the crack width in elements with varying bond properties.

- For hybrid reinforced concrete, some models have been suggested for the calculation of crack width for load-induced cracks, which are based on modifications of existing models for conventionally reinforced concrete. However, few models could be found in the literature for the calculation of crack width in hybrid reinforced concrete elements subjected to restraint cracking.

- The experimental tests carried out showed the beneficial effect of fibre reinforcement on the post-cracking behaviour of concrete. Based on the uniaxial tensile tests, increasing the fibre content from 0.25% to 1.0% vol., increased the residual tensile strength of the concrete from approximately $0.1f_{ct}$ to $0.8f_{ct}$ for crack width openings below 1 mm. This increase of the residual tensile strength resulted in a reduction of the mean crack width in RC tie elements, of up to 55%. On the other hand, the short-embedment pullout tests reveal that fibres had no effect on the bond behaviour in the pre-peak branch.

- An existing model, based on an analytical expression between the average crack width and the stress at the reinforcement, has been further developed by incorporating the effect of fibre reinforcement in order to obtain a new model able to predict the crack width in hybrid reinforced concrete elements subjected to restraint cracking.

- The proposed analytical expression that relates the average crack width with stress at the reinforcement agrees well with the average results from the experimental tests on RC tie elements as well as with other analytical formulations. However, it should be noted that

for the experimental results, a large scatter was found between individual cracks, particularly at high steel stresses.

- A comparison between different bond-slip relationship for the analytical expression used to calculate the crack width as a function of steel stress indicated that the most relevant part of the bond-slip relationship is for slips of up to 0.2 mm. Moreover, a good agreement was observed in the mentioned slip range between the expression provided in the Model Code 2010 and the experimental pullout test results.

- The present restraint cracking model was able to accurately predict the number of cracks formed in slabs experimentally tested by others. Moreover, a reasonable agreement was found between the analytical predictions and the experimental results for the average crack width and the maximum stress at the reinforcement, demonstrating the predictive capabilities of the model.

6.2. Suggestions for further research

To date, multiple experimental tests can be found in the literature where the effect of fibres on the crack width and crack spacing in RC tie elements are investigated for load-induced cracking. However, experimental tests for restraint cracking in hybrid reinforced concrete elements are lacking. Therefore, there is a clear need for further research on this topic.

The bond-slip relationship proposed in the Model Code 2010 is intended for anchorage calculations, i.e. ultimate limit state. Given the importance of describing the bond-slip relationship accurately at small slips for the calculation of the crack width, a thorough investigation should be carried out to assess the capability of the mentioned expression to reproduce the experimental behaviour of available pullout test results at small slips.
The proposed restraint cracking model for hybrid reinforced concrete elements, in its current state, is formulated in terms of the residual tensile strength. This implies that material characterization tests are required to determine this parameter and normally this is done by conducting flexural beam tests and converting the result to residual strength. Ideally, an expression could be developed to formulate the model in terms of the fibre characteristics, the dosage and orientation factor, which would avoid the need of experimental tests.

Furthermore, the restraint cracking model proposed in the present work could only be validated for a limited number of tests exclusively comprised of RC elements. Therefore, in addition to a further validation against results for complementary RC experiments, the validation for hybrid reinforced concrete elements is still required.

In addition, it would be beneficial to also examine and evaluate different reinforcement solutions for different crack width requirements and the associated production cost and life-cycle cost (LCC). Hence, to get a basis for the economic feasibility and potential of hybrid reinforcement solutions.

References

[1] L. Johansson, "Lärdomar från 30 års golvutredningar," Sammanfattningar, CBI:s informationsdag, 2003.

[2] G. Vitt, Combined reinforcement - practical experiences, in: 7th RILEM Int. Symp. Fibre Reinf. Concr. Des. Appl. - BEFIB 2008, 2008: pp. 1021–1028.

[3] B. Engström, Ductility of tie connections in precast structures, Doctoral thesis, Chalmers University of Technology, 1992.

[4] I. Löfgren, Calculation of crack width and crack spacing, in: Nord. Mini-seminar "Fibre Reinfroced Cocnrete," 2007.

[5] Svenska Betongföreningen, Betongrapport nr 13, Industrigolv - Rekommendationer för projektering, materialval, produktion, drift och underhåll, 2009.

[6] B. Engström, Restraint cracking of reinforced concrete structures, Undervisningmaterial Institutionen för bygg- & miljöteknik, Chalmers tekniska högskola, 2006.

[7] A. Ghali, R. Favre, M. Elbadry, Concrete Structures - Stresses and deformations, 3rd ed., Spon Press, 1986.

[8] R.I. Gilbert, G. Ranzi, Time-dependent behaviour of concrte structures, Spon Press, 2011.

[9] L. Östlund, Chapter 2 - Assumptions in design (Kapitel 2 - Förutsättningar för dimensionering), in: Betonghandb. - Konstr., 1990: pp. 51–88.

[10] I. Löfgren, Calculation of crack width and crack spacing, in: Nord. Mini-seminar "Fibre Reinfroced Cocnrete," Trondheim, Norway, 2007.

[11] ACI Committee 224, ACI 224R-01 Control of Cracking in Cocnrete Structures, 2001.

[12] I. Löfgren, Fibre-reinforced concrete for industrial construction - a fracture mechanics approach to material testing and structural analysis, Chalmers University of Technology, 2005.

[13] H. Stang, V.C. Li, Classification of fiber reinforced cementitious materials for structural applications, in: 6th RILEM Symp. Fiber-Reinforced Concr. - BEFIB 2004, 2004: pp. 197–218.

[14] E. Nordström, Durability of Sprayed Concrete Steel fibre corrosion in cracks, Luleå University of Technology, 2005.

[15] A. de la Fuente, P. Pujadas, A. Blanco, A. Aguado, Experiences in Barcelona with the use of fibres in segmental linings, Tunn. Undergr. Sp. Technol. 27 (2012) 60–71. doi:10.1016/j.tust.2011.07.001.

[16] D. Fall, Steel Fibres in Reinforced Concrete Structures of Complex Shapes, Chalmers University of Technology, Gothenburg, Sweden, 2014.

[17] Å. Døssland, Fibre Reinforcement in Load Carrying Concrete Structures, Norwegian University of Science and Technology, 2008.

[18] A. Marini, G. Plizzari, C. Zanotti, Seismic enhancement of existing buildings by means of fiber reinforced concrete diaphragms, Improv. Seism. Perform. Exist. Build. Other Struct. - Proc. 2009 ATC SEI Conf. Improv. Seism. Perform. Exist. Build. Other Struct. 4 (2009). doi:10.1061/41084(364)127.

[19] A. Bentur, S. Mindess, Fibre reinforced cementitious composites, 2nd ed., Taylor & Francis, Abingdon, United Kingdom, 2007.

[20] A. Blanco, Characterization and modelling of SFRC elements, Universitat Politècnica de Catalunya, 2013.

[21] M. Di Prisco, G. Plizzari, L. Vandewalle, Fibre reinforced concrete: new design perspectives, Mater. Struct. 42 (2009) 1261–1281. doi:10.1617/s11527-009-9529-4.

[22] P.H. Bischoff, Tension Stiffening and Cracking of Steel Fiber-Reinforced Concrete, J. Mater. Civ. Eng. 15 (2003) 174–182. doi:10.1061/(ASCE)0899-1561(2003)15:2(174).

[23] J. Cairns, G.A. Plizzari, Bond of Reinforcement in Fibre Reinforced Concrete, in: 6th RILEM Symp. Fibre-Reinforced Cocnretes - BEFIB 2004, Verenna, Italy, 2004: pp. 321–330.
[24] L. Vandewalle, Cracking behaviour of concrete beams reinforced with a combination of ordinary reinforcement and steel fibers, Mater. Struct. 33 (2000) 164–170. doi:10.1007/BF02479410.
[25] A. Jansson, Effects of Steel Fibres on Cracking in Reinforced Concrete, PhD thesis - Chalmers University of Technology, Gothenburg, Sweden, 2011.
[26] K. Noghabai, Behavior of Tie Elements of Plain and Fibrous Concrete and Varying Cross Sections, ACI Struct. J. 97 (2000) 277–285. doi:10.14359/857.
[27] J. Deluce, S. Lee, F.J. Vecchio, Crack Formation in FRC Structural Elements Containing Conventional Reinforcement, in: A.E. Parra-Montesinos, GustavoJ. and Reinhardt, HansW. and Naaman (Ed.), High Perform. Fiber Reinf. Cem. Compos. 6, Vol. 2 - RILEM State Art Reports, 2012: pp. 271–278. doi:10.1007/978-94-007-2436-5_33.
[28] L.H. Lárusson, Development of Flexible Link Slabs using Ductile Fiber Reinforced Concrete, Technical University of Denmark, Lyngby, Denmark, 2013.
[29] A. Solgaard, A. Michel, M. Geiker, H. Stang, Concrete cover cracking due to uniform reinforcement corrosion, Mater. Struct. (2013) 1–19. doi:10.1617/s11527-013-0016-6.
[30] N. Görander, C. Halldén, Crack Width Profiles for Fibre- reinforced Concrete Elements with Conventional Reinforcement, Göteborg, Sweden, 2015.
[31] C.G. Berrocal, I. Löfgren, K. Lundgren, N. Görander, C. Halldén, Characterisation of bending cracks in R/FRC using image analysis, Cem. Concr. Res. 90 (2016) 104–116. doi:10.1016/j.cemconres.2016.09.016.
[32] C.G. Berrocal, I. Löfgren, K. Lundgren, L. Tang, Corrosion initiation in cracked fibre reinforced concrete: Influence of crack width, fibre type and loading conditions, Corros. Sci. (2015). doi:10.1016/j.corsci.2015.05.021.
[33] S. Persson, T. Kanstad, Ø. Bjøntegaard, B. Pedersen, A. Vatnar, E.L. Skare, Bruk av fiberbetong i kantdrager, 11-2427 Sandsgård gang- og sykkelbru, 2017.
[34] EN 1992-1-1 Eurocode 2, EN 1992-1-1 Eurocode 2: Design of concrete structures - Part 1-1: General rules and rules for buildings, (2004).
[35] Model Code, fib Model Code for Concrete Structures, Wiley-VCH Verlag GmbH & Co. KGaA, Weinheim, Germany, 2010. doi:10.1002/9783433604090.
[36] RILEM TC 162-TDF, σ-ε - design method - Final Recommendation, Mater. Struct. 36 (2003) 560–567.
[37] K. Moffatt, Analyse de Dalles de Pont avec Armature Réduite et Béton de Fibres Metalliques, MscA thesis, École Polytechnique de Montréal, QC, Canada, 2001.
[38] M. Gustafsson, S. Karlsson, Fiberarmerade betongkonstruktioner – Analys av sprickavstånd och sprickbredd (Fibre-reinfroced concrete - Analysis of crack spacing and crack width), Examensarbete Chalmers Tekniska Högskola, Rapport:2006:105, 2006.
[39] R.D. Jordon, L. Seong-Cheol, F.J. Vecchio, Crack model for steel fiber-reinforced concrete members containing conventional reinforcement, ACI Struct. J. 111 (2014) 93–102. doi:10.14359/51686433.
[40] Comité Euro International du Béton (CEB/FIP), Model Code for Concrete Structures, CEB-FIP International Recommendations, Paris, France, 1978.
[41] British Standard Institution, BS 8007:87 Design of concrete structures for retaining aqueous liquids, London, UK, 1987.
[42] R. Nejadi, R.I. Gilbert, Shrinkage Cracking in Restrained Reinforced Concrete Members, Volume 433 of UNICIV report - University of New South Wales. School of Civil Engineering, 2004.

[43] U. Häubler-Combe, J. Hartig, Evaluation of concrete cracking due to restrained thermal loading and shrinkage, ACI Struct. J. 109 (2012) 41–52.
[44] CEB-FIP, High Performance Concrete - Recommended Extensions to the Model Code 90 and Research Needs, Bulletin d'Information No. 228, Lausanne, July 1995, 1995.
[45] Comite Euro-International Du Beton, CEB-FIP Model Code 1990: Design Code, in: CEB-FIP Model CODE 1990, Thomas Telford Publishing, 1993: pp. i–xxii. doi:10.1680/ceb-fipmc1990.35430.fm.
[46] N. Tue, G. König, Calculating the mean bon and steel stress in reinforced and prestressed concrete members, Darmstadt Concr. 6 (1991) 77–86.
[47] C.G. Berrocal, I. Fernandez, K. Lundgren, I. Löfgren, Corrosion-induced cracking and bond behaviour of corroded reinforcement bars in SFRC, Compos. Part B Eng. (2017). doi:10.1016/j.compositesb.2017.01.020.
[48] K. Lundgren, I. Lofgren, A. Jansson, K. Gylltoft, Bond of reinforcement in self-compacting steel-fibre-reinforced concrete, Mag. Concr. Res. 64 (2012) 617–630. doi:10.1680/macr.11.00091.
[49] A. Jansson, I. Lofgren, K. Lundgren, K. Gylltoft, Bond of reinforcement in self-compacting steel-fibre-reinforced concrete, Mag. Concr. Res. 64 (2012) 617–630. doi:10.1680/macr.11.00091.
[50] RILEM TC 162-TDF, Recommendations of RILEM TC 162-TDF: Test and design methods for steel fibre reinforced concrete Uni-axial tension test for steel fibre reinforced concrete, Mater. Struct. 34 (2005) 3–6. doi:10.1617/13628.
[51] P. Niemann, Gebrauchsverhalten von Betonbauteilen aus Stahlfaserbeton mit Betonstahlbewehrung, Institut für Baustoffe, Massivbau und Brandschutz (iBMB), Braunschweig - Germany, 2001.